

PROPERTIES OF POLYLACTIDE / MONTMORILLONITE
NANOCOMPOSITES: BEFORE AND AFTER WEATHERING

A THESIS SUBMITTED TO
THE GRADUATE SCHOOL OF NATURAL AND APPLIED SCIENCES
OF
MIDDLE EAST TECHNICAL UNIVERSITY

BY

BURCU SARI

IN PARTIAL FULFILLMENT OF THE REQUIREMENTS
FOR
THE DEGREE OF MASTER OF SCIENCE
IN
POLYMER SCIENCE AND TECHNOLOGY

AUGUST 2015

Approval of the thesis:

**PROPERTIES OF POLYLACTIDE / MONTMORILLONITE
NANOCOMPOSITES: BEFORE AND AFTER WEATHERING**

submitted by **BURCU SARI** in partial fulfillment of the requirements for the degree of **Master of Science in of Polymer Science and Technology Department, Middle East Technical University** by,

Prof. Dr. Gülbin Dural Ünver
Dean, **Graduate School of Natural and Applied Sciences**

Prof. Dr. Necati Özkan
Head of Department, **Polymer Science and Technology**

Prof. Dr. Cevdet Kaynak
Supervisor, **Metallurgical and Materials Eng. Dept., METU**

Examining Committee Members:

Prof. Dr. Göknur Bayram
Chemical Engineering Dept., METU

Prof. Dr. Cevdet Kaynak
Metallurgical and Materials Engineering Dept., METU

Assoc. Prof. Dr. H. Emrah Ünalın
Metallurgical and Materials Engineering Dept, METU

Assist. Prof. Dr. İrem Erel Göktepe
Chemistry Dept., METU

Assist. Prof. Dr. Metehan Erdoğan
Materials Engineering Dept., Yıldırım Beyazıt University

DATE: 27.08.2015

I hereby declare that all information in this document has been obtained and presented in accordance with academic rules and ethical conduct. I also declare that, as required by these rules and conduct, I have fully cited and referenced all material and results that are not original to this work.

Name, Last Name : Burcu Sari

Signature :

ABSTRACT

PROPERTIES OF POLYLACTIDE / MONTMORILLONITE NANOCOMPOSITES: BEFORE AND AFTER WEATHERING

Sari, Burcu

M. S., Department of Polymer Science and Technology

Supervisor: Prof. Dr. Cevdet Kaynak

August 2015, 93 pages

The aim of the first part of thesis was to investigate the effects of montmorillonite (MMT) type nanoclay content and maleic anhydride (MA) grafted polylactide (PLA) copolymer compatibilization on the properties of PLA nanocomposites. Nanocomposites have compounded by twin-screw extrusion melt-mixing followed with injection molding for shaping of bulk specimens. Successively intercalated and exfoliated structures of the nanocomposites were observed by XRD and TEM analysis, including the interactions with FTIR. Mechanical tests indicated that use of only 1 wt% MMT resulted in significant improvements in many mechanical properties of PLA. Increases were only 14% in flexural modulus and 6% in flexural strength, but more than 6 times in ductility and as much as 85% in fracture toughness values. After MA compatibilization these improvements were higher, being more than 22 times in ductility and 119% in fracture toughness. On the other hand, no significant changes in the transition temperatures and thermal degradation temperatures of PLA were observed in DSC and TGA thermal analyses.

The aim of the second part of this thesis was to compare accelerated weathering performance of neat PLA and its 1 wt% organically modified MMT nanocomposite. Accelerated weathering test system applied consecutive steps of UV irradiation and humidity in accordance with ISO 4892-3 standards for 200 hours. Chain scission actions of weathering degradation mechanisms photolysis, photooxidation and hydrolysis resulted in significant decrease in the molecular weight of PLA; consequently certain reductions in the modulus, strength, ductility and toughness of the specimens. However, it can be deduced that, after comparing mechanical properties of PLA and PLA/MMT before and after 200 h accelerated weathering, use of PLA with only 1 wt% MMT was extremely beneficial not only for “indoor applications” but also for “outdoor applications”. For example, the benefit gained in flexural strength was 6% before weathering, but after weathering the benefit gained was 88%. The reasons of this increments are the effective reinforcing and barrier actions of intercalated/exfoliated MMT layers.

Key words: Polylactide, Montmorillonite, Nanocomposite, Maleic Anhydride, Interfacial Compatibilization, Accelerated Weathering

ÖZ

POLİLAKTİT / MONTMORİLLONİT NANOKOMPOZİTLERİN ATMOSFERİK YAŞLANMA ÖNCESİ VE SONRASI ÖZELLİKLERİ

Sarı, Burcu

Yüksek Lisans, Polimer Bilim ve Teknolojisi Bölümü

Tez Yöneticisi: Prof. Dr. Cevdet Kaynak

Ağustos 2015, 93 sayfa

Tezin birinci bölümünün amacı montmorillonit (MMT) tipi nanokil miktarının ve maleik anhidrit (MA) ile graft edilmiş polilaktid (PLA) kopolimer uyumlaştırmasının PLA/MMT nanokompozitlerinin özellikleri üzerindeki etkisini incelemektir. Nanokompozitler çift vidalı ekstrüder eriyik karıştırma yöntemi ile kompaund edilmiş, ardından enjeksiyon kalıplama yöntemi ile şekil verilmiştir. Nanokompozitlerin interkale ve eksfoliye yapıları XRD ve TEM analizleri ile, kimyasal etkileşimleri ise FTIR ile gözlenmiştir. Mekanik testler ağırlıkça %1 MMT kullanımının PLA'nın birçok mekanik özelliğinde önemli artışlara neden olduğunu göstermiştir. Artışlar eğme modülünde ve mukavemetinde sadece %14 ve %6 iken, süneklik değerinde 6 katın üzerinde, kırılma tokluğunda ise %85'e varan artışlar olmuştur. MA uyumlaştırmasından sonra bu artışlar çok daha büyük oranlarda, örneğin süneklik değerinde 22 katın üzerinde, kırılma tokluğunda ise %119 olmuştur. Diğer yandan, DSC ve TGA analizlerinde PLA'nın ısıl dönüşüm ve ısıl degradasyon sıcaklıklarında önemli bir değişim olmadığı gözlemlenmiştir.

Tezin ikinci bölümünün amacı ise saf PLA ve onun ağırlıkça %1 MMT nanokompozitinin hızlandırılmış atmosferik yaşlandırma altındaki performanslarını karşılaştırmaktır. Hızlandırılmış atmosferik yaşlandırma test sistemi ISO 4892-3 standardı ile uyumlu toplam 200 saat ardışık UV radyasyonu ve nem döngüleri

uygulamıştır. Atmosferik deęredasyon mekanizmaları fotoliz, fotooksidasyon ve hidrolizin zincir kesme etkileri PLA'nın moleköl aęırlıęında önemli azalmalara, dolayısıyla da numunelerin modöl, mukavemet, süneklik ve tokluk deęerlerinde belli oranlarda düşüşlere neden olmuştur. Ancak, PLA ve PLA/MMT numunelerinin 200 saatlik atmosferik yaşlandırma öncesi ve sonrası mekanik özellikleri karşılaştırıldığında, aęırlıkça %1 MMT içeren PLA kullanımının yalnızca “iç mekân uygulamaları” için deęil aynı zamanda “dış mekân uygulamaları” için de oldukça yararlı, kazançlı olduęu sonucu çıkarılabilir. Örneęin, eęme mukavemetinde elde edilen kazanç yaşlandırma öncesinde %6 iken yaşlandırma sonrasındaki kazanç %88 olmuştur. Bunun nedeni, interkale/eksfolye MMT katmanlarının sahip olduęu oldukça etkili takviye ve bariyer nitelikleridir.

Anahtar Kelimeler: Polilaktid, Montmorillonit, Nanokompozit, Maleik Anhidrit, Arayüzey Uyumlaştırması, Hızlandırılmış Atmosferik Yaşlandırma

to 3 or 5 trees of the #GeziPark

ACKNOWLEDGEMENTS

First of all I would like to express my deepest gratitude to my supervisor Prof. Dr. Cevdet Kaynak for not only his criticism, tolerance and insight throughout the research; but also, his human face in the academic world and his encouragements.

I would like to thank to the members of the examining committee, Prof. Dr. Gökür Bayram, Assoc. Prof. Dr. Hüsnü Emrah Ünalın, Assist. Prof. Dr. İrem Erel Göktepe and Assist. Prof. Dr. Metehan Erdoğan for their valuable discussion and contribution during my thesis defense period.

I would also like to acknowledge the administrative board and all the technical staff of the Metallurgical and Materials Engineering Department for supplying all the research facilities required in this dissertation. I am especially grateful to Önder Şahin, Nilüfer Özel and Serkan Yılmaz for their invaluable help.

I want to thank my laboratory mates, Berk Dođu, Yelda Meyva, Ali Rıza Erdoğan and Deniz Varsavas for their friendship and support. I am so lucky to have such brilliant people around me.

I am also thankful to all my friends with whom I tried to colorize the moments of this monochrome world. This dissertation would certainly be not possible without their support. Merve Uzuner's, Erim Alkan's and Mert Kükürer's encouragements provided with me keep up with the study.

I am indebted to my family who has always supported all my decisions throughout my life even if they were wrong. I am also grateful to my dear sister Beste Nur Sarı who is a great gift to me.

TABLE OF CONTENTS

ABSTRACT	v
ÖZ	vii
ACKNOWLEDGEMENTS	x
TABLE OF CONTENTS	xi
LIST OF TABLES	xiii
LIST OF FIGURES	xv
NOMENCLATURE	xviii
CHAPTERS	1
1. INTRODUCTION	1
1.1 Polylactide	1
1.2 Montmorillonite.....	6
1.3 Polymer/Montmorillonite Nanocomposites	8
1.4 Weathering Degradation of PLA	15
1.5 Literature Survey	15
1.5.1 Previous Studies on the Behavior of PLA/MMT Nanocomposites	15
1.5.2 Previous Studies on the Interfacial Compatibilization of the PLA/MMT Nanocomposites.....	16
1.5.3 Previous Studies on the Accelerated Weathering Behavior of PLA based Nanocomposites.....	17
1.6 Purpose of the Study.....	19
2. EXPERIMENTAL WORK	21
2.1 Materials Used.....	21
2.2 Production of PLA/MMT Nanocomposites	22
2.3 Production of PLA/gMA/MMT Nanocomposite	23
2.4 Structural Characterization by XRD, TEM, FTIR and SEM	23
2.5 Mechanical Tests and Thermal Analyses	24

2.6	Accelerated Weathering of the Neat PLA and its PLA/MMT Nanocomposite	25
2.7	Changes in the MMT Intercalation and PLA Crystallinity	26
2.8	Changes in the Color of the Specimens	26
2.9	Changes in the Chemical Structure of the Specimens	26
2.10	Changes in the Fracture Surface Morphology, Mechanical Properties and Thermal Behavior of Specimens	27
3.	RESULTS AND DISCUSSION.....	29
3.1	Effects of MMT Content and MA Compatibilization	29
3.1.1	Intercalated Structure of the PLA/MMT Nanocomposites	29
3.1.2	Chemical Structure of PLA/MMT Nanocomposites.....	32
3.1.3	Modulus and Strength of the PLA/MMT Nanocomposites	34
3.1.4	Ductility and Toughness of the PLA/MMT Nanocomposites	38
3.1.5	Thermal Properties of the PLA/MMT Nanocomposites	45
3.2	Effects of Accelerated Weathering.....	49
3.2.1	Effects on the MMT Intercalation	50
3.2.2	Effects on the PLA Crystallization.....	52
3.2.3	Effects on in the Color	54
3.2.4	Effects on the Chemical Structure.....	57
3.2.5	Effects on the Fracture Surface Morphology	61
3.2.6	Effects on the Mechanical Properties.....	62
3.2.7	Effect on the Thermal Behavior	72
4.	CONCLUSIONS.....	78
	REFERENCES.....	82

LIST OF TABLES

TABLES

Table 3.1 Flexural modulus (E_{Flex}), tensile modulus (E), flexural strength (σ_{Flex}) and tensile strength (σ_{TS}) values of the specimens	36
Table 3.2 Tensile strain at break (ϵ_f) and fracture toughness (K_{IC} and G_{IC}) of the specimens.....	41
Table 3.3 Transition temperatures (T_g , T_c , T_m), enthalpies (ΔH_m , ΔH_c) and crystallinity percent (X_C) of the specimens during first heating profile.....	47
Table 3.4 Thermal degradation temperatures ($T_{5\%}$, $T_{10\%}$, $T_{25\%}$) of the specimens at 5, 10 and 25 wt% mass losses and the maximum mass loss temperature (T_{max}).....	48
Table 3.5 Effects of accelerated weathering periods on the CIELAB color space parameters (L^* , a^* , b^*) and color change difference (ΔE^*) values of the specimens.....	56
Table 3.6 Effects of accelerated weathering periods on the Flexural Modulus (E_{Flex}), Tensile Modulus (E), Flexural Strength (σ_{Flex}) and Tensile Strength (σ_{TS}) of the specimens	62
Table 3.7 Effects of accelerated weathering periods on the tensile strain at break (ϵ_f) and fracture toughness (K_{IC} and G_{IC}) of the specimens.....	68
Table 3.8 Comparison of the mechanical properties of neat PLA and PLA/MMT nanocomposite specimens before (0 h) and after (200 h) accelerated weathering, including the “% benefit” (percent increase in the values) of the nanocomposite specimen at 0 h and 200 h.....	71
Table 3.9 Effects of accelerated weathering periods on the transition temperatures (T_g , T_c , T_m), enthalpies (ΔH_m , ΔH_c) and crystallinity percent (X_C) of the specimens..	74

Table 3.10 Effects of accelerated weathering periods on the thermal degradation temperatures ($T_{5\%}$, $T_{10\%}$, $T_{25\%}$) of the specimens at 5, 10 and 25 wt% mass losses and the maximum mass loss temperature (T_{max})76

LIST OF FIGURES

FIGURES

Figure 1.1 Chemical structure of PLA.....	2
Figure 1.2 Structures of L-, D- and DL-lactic acids and lactides.....	2
Figure 1.3 Synthesis methods for high molecular weight PLA.....	3
Figure 1.4 Projection of proposed orthorhombic unit cell of PLA α -crystal structure on the ab plane. Full circles: carbon atoms; dotted circles: oxygen atoms.....	4
Figure 1.5 Proposed chain conformation of the orthorhombic PLA α -crystal structure	5
Figure 1.6 Structure of montmorillonite.....	7
Figure 1.7 Organic modification of montmorillonite	8
Figure 1.8 Illustration of different types of composite that can arise from the interaction between layered silicates and polymers. (a) Phase-separated composite (microcomposite). (b) Intercalated composite (nanocomposite). (c) Exfoliated composite (nanocomposite)	9
Figure 1.9 Proposed Norrish type II photocleavage reaction for PLA	11
Figure 1.10 Plausible photodegradation mechanisms occurring in PLA. Mechanism (a): photolysis reaction inducing a cleavage of the backbone C–O bond. Mechanism (b): photooxidation of PLA leading to the formation of hydroperoxide derivatives..	12
Figure 1.11 Radical oxidation process of UV irradiated PLA samples: Hydroperoxide chain propagation and formation of anhydrides by photolysis of hydroperoxide	13
Figure 1.12 Possible hydrolysis reaction of PLA.....	14
Figure 3.1 XRD Patterns of the organically modified MMT and PLA/MMT Nanocomposites.....	30
Figure 3.2 TEM images showing (a) and (b) uniform distribution, (c) and (d) intercalation and exfoliation of MMT layers in PLA matrix.....	31
Figure 3.3 ATR-FTIR spectra of neat PLA and PLA/MMT nanocomposites	33

Figure 3.4 Stress-strain curves of the specimens obtained during three point bending flexural and tensile tests.....	35
Figure 3.5 Effects of MMT content and MA compatibilization on the modulus and strength of the specimens (note that gMA in the <i>x</i> -axes denotes PLA/gMA/MMT 1 specimen)	37
Figure 3.6 Effects of MMT and PLA-g-MA compatibilization on the ductility of the specimens in terms of tensile elongation at break.....	39
Figure 3.7 Effects of MMT content and MA compatibilization on the ductility (ϵ_f) and fracture toughness (K_{IC} and G_{IC}) of the specimens (note that gMA in the <i>x</i> -axes denotes PLA/gMA/MMT 1 specimen)	42
Figure 3.8 SEM fractographs showing fracture surface morphology of neat PLA and PLA/MMT nanocomposites.....	44
Figure 3.9 First heating DSC thermograms of the specimens.....	46
Figure 3.10 . Thermogravimetric (TG) curves of the specimen	49
Figure 3.11 Effects of accelerated weathering periods on the XRD diffractograms showing intercalated nanocomposite structure, including TEM images of the intercalated and exfoliated MMT layers.....	51
Figure 3.12 Effects of accelerated weathering periods on the XRD diffractograms of the specimens showing PLA crystallization.....	53
Figure 3.13 Effects of accelerated weathering periods on the photographic images of the specimens showing slight variation in the color	55
Figure 3.14 Effects of accelerated weathering periods on the ATR-FTIR spectra of the specimens showing variation in the chemical structure	58
Figure 3.15 Effects of accelerated weathering periods on the SEM images of the specimens showing variation in the fracture surface morphology.....	61
Figure 3.16 Effects of accelerated weathering periods on the flexural stress-strain curves of the specimens.....	63
Figure 3.17 Effects of accelerated weathering periods on the tensile stress-strain curves of the specimens.....	64
Figure 3.18 Effects of accelerated weathering periods on the flexural and tensile modulus, and flexural and tensile strength of the specimens.....	66

Figure 3.19 Effects of accelerated weathering periods on the ductility and fracture toughness of the specimens.....	70
Figure 3.20 Effects of accelerated weathering periods on the first heating DSC thermograms of the specimens.....	73
Figure 3.21 Effects of accelerated weathering periods on the thermogravimetric curves of the specimens.....	77

NOMENCLATURE

2θ	:	XRD diffraction angle
σ_{TS}	:	tensile strength
σ_{Flex}	:	flexural strength
ε_f	:	elongation at break, final strain
ΔH_m	:	melting enthalpy of the specimens
ΔH_c	:	crystallization enthalpy of the specimens
ΔH_m^\bullet	:	melting enthalpy of 100% crystalline PLA
E	:	tensile modulus
E_{Flex}	:	flexural modulus
G_{Ic}	:	fracture toughness as critical strain energy release rate
K_{Ic}	:	fracture toughness as critical stress intensity factor
$T_{5wt\%}$:	thermal degradation temperature at 5 wt% mass loss
$T_{10wt\%}$:	thermal degradation temperature at 10 wt% mass loss
$T_{25wt\%}$:	thermal degradation temperature at 25 wt% mass loss
T_c	:	cold crystallization temperature
T_g	:	glass transition temperature
T_m	:	melting temperature
T_{max}	:	thermal degradation temperature at maximum mass loss rate
X_c	:	degree of crystallinity
w_{PLA}	:	weight fraction of PLA
ATR-FTIR	:	attenuated total reflectance-Fourier transform infrared spectroscopy
DRA	:	diffused reflectance analysis

DSC	:	differential scanning calorimetry
MA	:	maleic anhydride
MMT	:	montmorillonite
PLA	:	poly(lactic acid) or polylactide
PLLA	:	L-enantiomer of polylactide
PDLA	:	D-enantiomer of polylactide
PLA-g-MA	:	maleic anhydride grafted polylactide
SEM	:	scanning electron microscopy
SLS	:	static light scattering spectroscopy
TGA	:	thermogravimetric analysis
XRD	:	X-ray diffraction
TEM	:	transmission electron microscopy

CHAPTER 1

INTRODUCTION

1.1 Polylactide

Compared to metals and ceramics, thermoplastic polymers possess optimal properties for use in packaging and many other consumer products, such as light weight, enhanced barrier properties and ease of shaping. Up to the present, polymers were mostly derived from non-renewable petroleum and natural gas resources. Recycling and reusing of petroleum-based polymers has many difficulties with respect to cost and processability. Over the past decade, increment in interest on biodegradable polymers derived from renewable sources have made inroads into solutions to diminish solid waste disposal problems and to decrease the dependency on petroleum and natural gas.

Poly(lactic acid) (PLA) is a biodegradable polymer derived from renewable sources such as starch and sugar. Until the last decade, the main uses of PLA have been limited to medical usages such as implants, tissue scaffolds, and internal sutures, because of its high cost, low availability and limited molecular weight. Recently, new techniques which allow economical production of high molecular weight PLA polymer have broadened its uses. Its low toxicity, along with its environmentally benign characteristics, has made PLA an ideal material for food packaging and for other consumer products [1]. The chemical structure of PLA with end groups is shown in Figure 1.1.

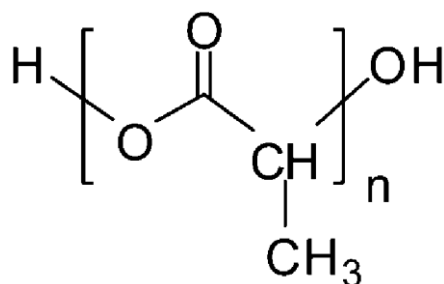


Figure 1.1 Chemical structure of PLA [2].

Lactic acid is the basic hydroxy acid with an asymmetric carbon atom existing in two active stereoisomers optically: L and D enantiomers as shown in Figure 1.2. Generally L- and D-lactic acids are synthesized via fermentation using micro-organisms. Racemic DL-lactic acid consists of equimolar mixture of L- and D-lactic acids and had different characteristics from those of the optically active ones. DL-lactic acid is favorably synthesized by chemical methods rather than fermentation [3].

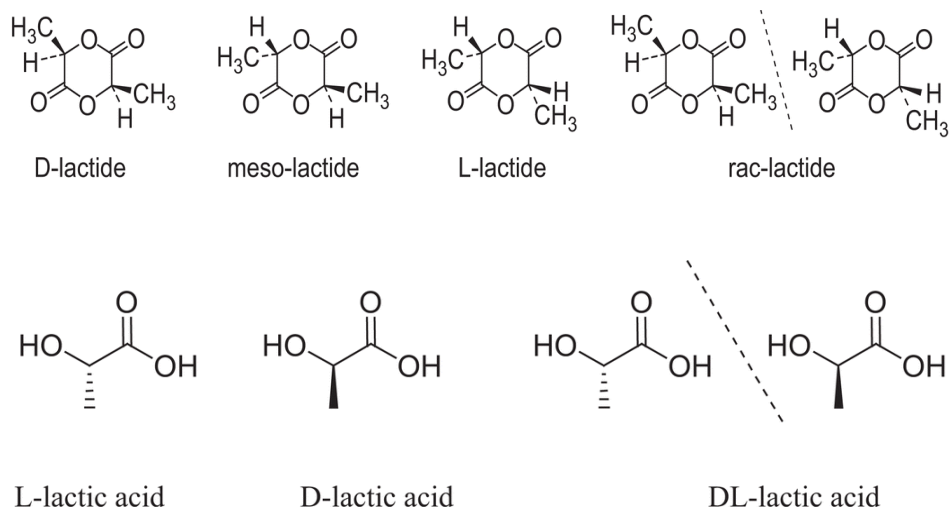


Figure 1.2 Structures of L-, D- and DL-lactic acids and lactides [3].

The synthesis of lactic acid into high-molecular weight PLA can follow two different routes of polymerization, as shown in Figure 1.3. The monomer lactic acid is condensation polymerized to yield a low-molecular weight, brittle, glassy polymer in the first route, which, for the most part, is unusable unless external coupling agents are used to increase the molecular weight of the polymer. The second route of producing PLA is to collect, purify, and ring-open and polymerize lactide to yield high molecular weight (average $M_w > 100,000$) PLA [4-5].

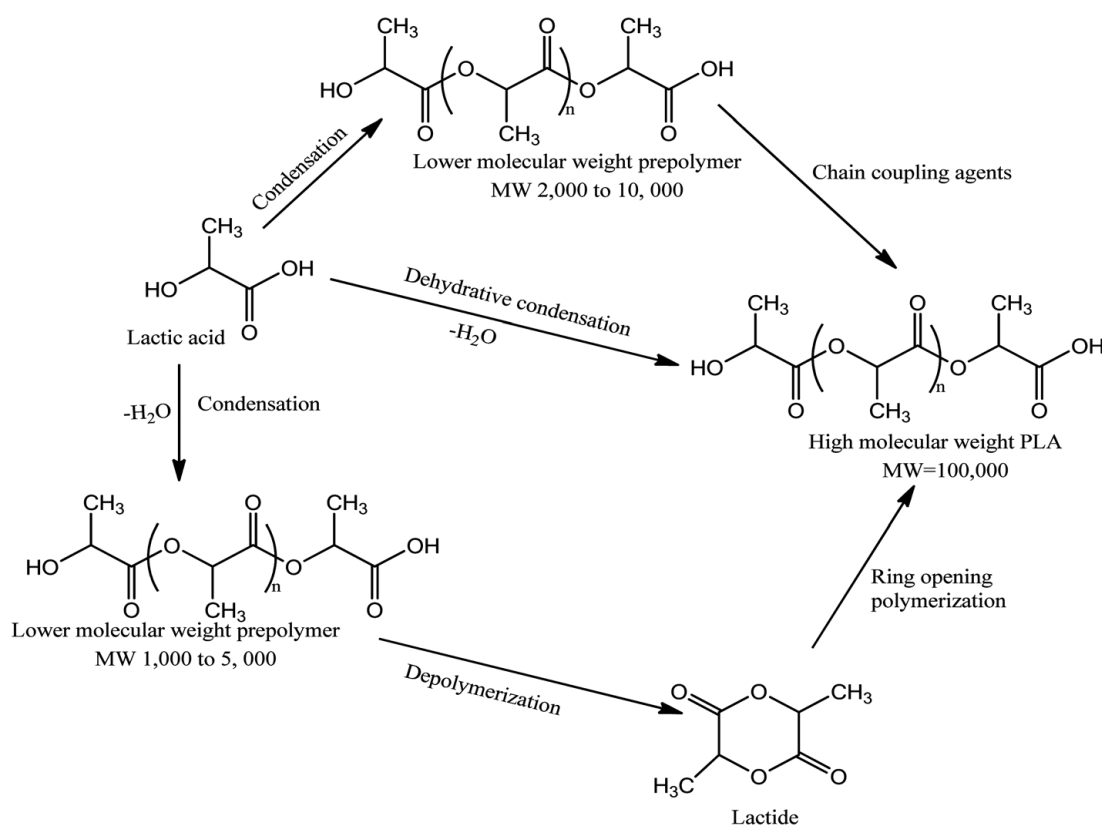


Figure 1.3 Synthesis methods for high molecular weight PLA [5].

PLA is a semicrystalline biopolymer, its most stable crystal structure is α phase. It can develop upon melt or cold crystallization, or from the solution. The proposed structure is orthorhombic, but the unit cell parameters are not well established. Projection of the proposed orthorhombic unit cell on ab plane is shown in Figure 1.4 [6], while a chain

model for the orthorhombic conformation is shown in Figure 1.5 [7]. The 2θ locations for α phase are observed at 16.3° and 18.7° assigned to (200/110) and (203) planes, respectively.

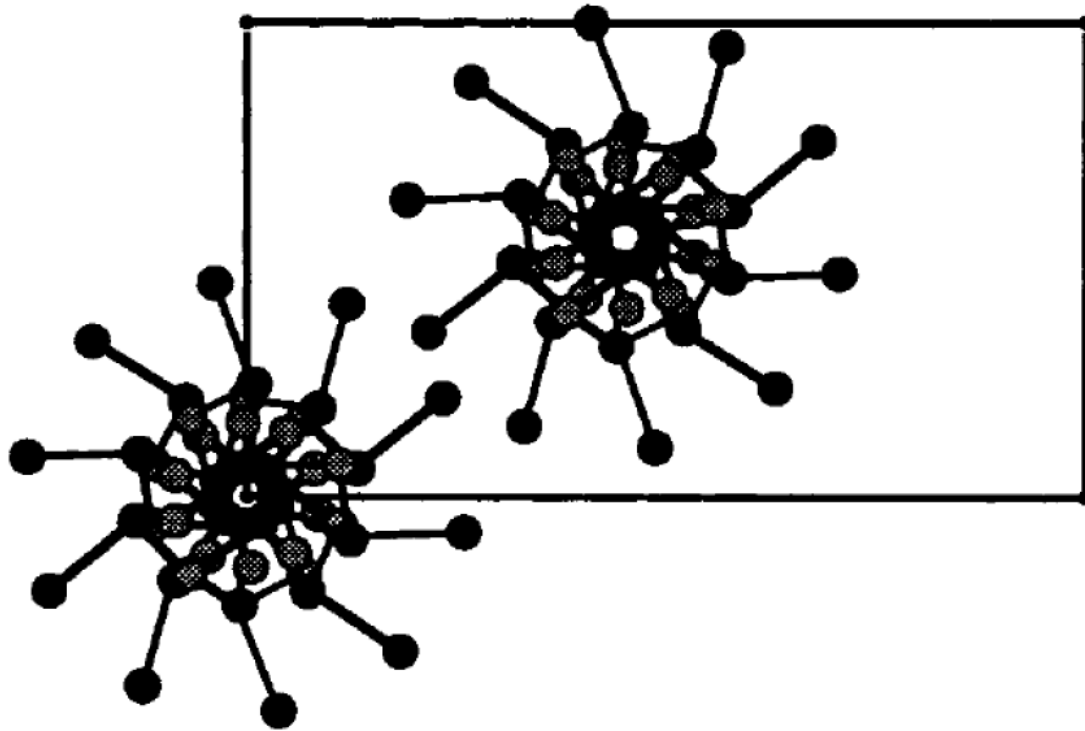


Figure 1.4 Projection of proposed orthorhombic unit cell of PLA α -crystal structure on the ab plane. Full circles: carbon atoms; dotted circles: oxygen atoms [6].

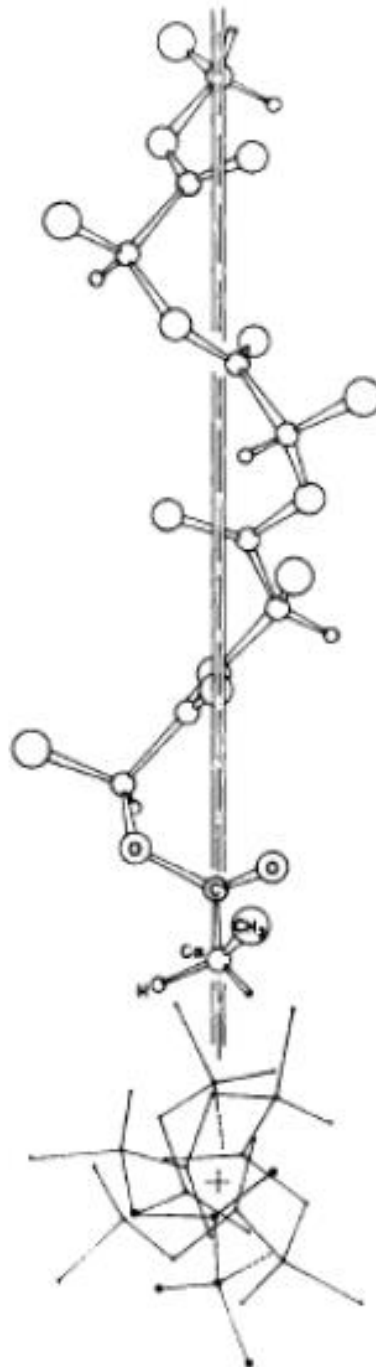


Figure 1.5 Proposed chain conformation of the orthorhombic PLA α -crystal structure [7].

Thermal and mechanical properties of PLA are mainly affected by molecular weight and optical purity. Commercially available L-lactic acid type PLA grades have glass transition temperature range of 55-60°C, melting temperature range of 130-230°C and thermal degradation temperature range of 240-260°C. Their flexural and tensile modulus range is 3-4 GPa, flexural strength range is 60-100 MPa, tensile strength range is 50-70 MPa, strain at break range is 2-4% and fracture toughness range is 2-4 MPa√m.

In the concept of “green” eco-friendly materials, PLA represents the best polymeric substitutes for various petro-polymers because of its renewability, biodegradability, biocompatibility and rather better thermomechanical properties compared to other biopolymers. Most of its applications are available for biomedical sector and short-time uses such as packaging, particularly due to the biodegradable properties of PLA. Interestingly, due to the depletion of petroleum resources, PLA is getting importance in long-term engineering applications such as automotive and electronics.

However, for such applications, PLA has some challenges such as brittleness and low values of thermal resistance, heat distortion temperature and rate of crystallization. These deficiencies can be overcome by adding nanofillers, such as montmorillonite.

1.2 Montmorillonite

Layered silicates have attracted the extreme interest in the last decade in academia and industry due to their dispersibility as the reinforcement material in polymeric matrices. It is also possible to adjust their surface chemistry by ion exchange reactions. The most common layered silicate mineral used for nanocomposite purpose is montmorillonite (MMT) a member of the 2:1 phyllosilicates family. MMT was discovered in 1848 in Montmorillon, France by Damour and Salvétat [8].

MMT has a theoretical formula of $(\text{OH})_4\text{Si}_8\text{Al}_4\text{O}_{20} \cdot n\text{H}_2\text{O}$ while its layered structure as shown in Figure 1.6 is composed of two tetrahedral sheets of silica surrounding an octahedral sheet of alumina or magnesia. Excess negative charges are formed by isomorphous substitutions of Si^{4+} and Al^{3+} in tetrahedral lattice and Al^{3+} for Mg^{2+} on octahedral sheet. Then, the negative charges are counterbalanced by cations such as Ca^{2+} and Na^+ taking place in between the layers. Hydrophilic character of MMT hold water molecules inside layers. Uniform van der Waals gaps between the plates are called as “interlayers” or “galleries”. Layer thickness together with interlayer represent the repeating unit of this multilayered structure which is known as “basal spacing” or “*d*-spacing”, in which varies from 1 nm to 30 nm [8].

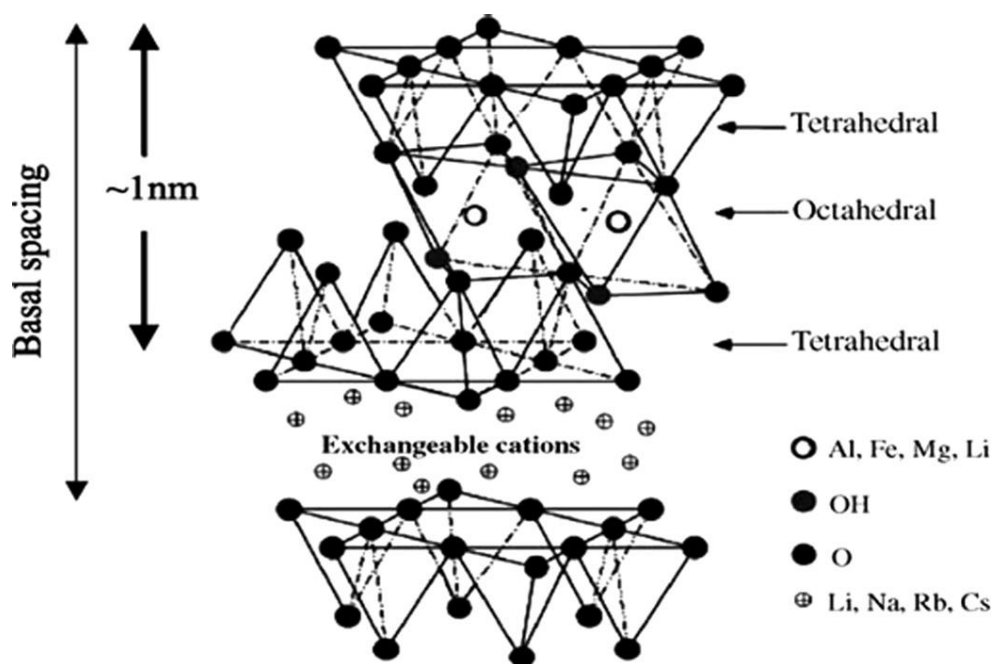


Figure 1.6 Structure of montmorillonite [8].

Since the montmorillonite layers consist of mostly silica and alumina, it has “hydrophilic” nature with a tendency of stack formation. Therefore, it is necessary to organically modify and make it “organophilic” in order to incorporate into polymer

matrices. This modification eases the transportation of polymer chains through the “galleries” and result in wider interlayer gap, which is called “intercalation”.

Organic modification of layered silicates is generally done by cation exchange reaction as shown in Figure 1.7. That is, inorganic cations (typically sodium) on the surface of the montmorillonite to balance the negative charge of aluminum/magnesium silicate layers, are placed with the organic cations (typically alkyl ammonium ions) so that the clay became organophilic.

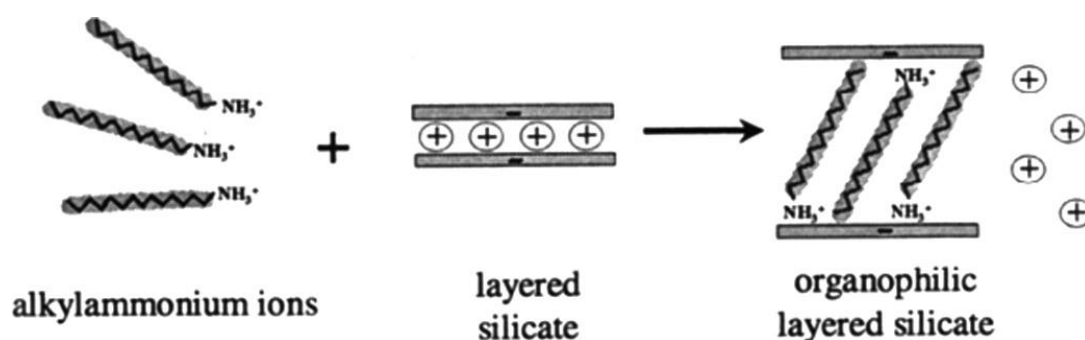


Figure 1.7 Organic modification of montmorillonite [8].

1.3 Polymer/Montmorillonite Nanocomposites

Improved properties of polymer/MMT nanocomposites over to conventional composites is provided by strong interfacial interactions of polymer and MMT. MMT particles having high aspect ratio disperse in a polymer matrix and create much higher surface area.

Depending on the structure of dispersed clay platelets in polymer matrix, the composites can be classified as microcomposite or intercalated/exfoliated nanocomposites [9].

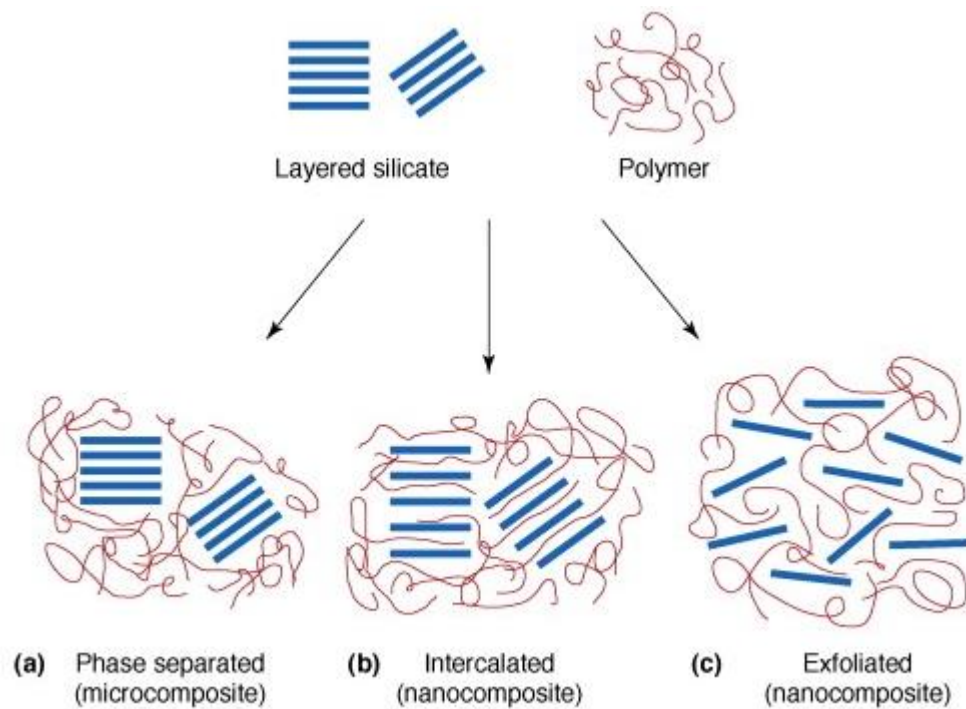


Figure 1.8 Illustration of different types of composite that can arise from the interaction between layered silicates and polymers. (a) Phase-separated composite (microcomposite). (b) Intercalated composite (nanocomposite). (c) Exfoliated composite (nanocomposite) [10].

When polymer chains can not enter clay galleries, due to poor polymer-clay interaction, “phase separated microcomposite” structure (Figure 1.8(a)) can be obtained.

“Intercalated nanocomposite” structures (Figure 1.8(b)) are self-assembled, well-ordered multilayered structures where the polymer chains are diffused into the galleries of the MMT. This leads to an opening of the interlayer d -spacing.

“Exfoliated nanocomposite” structure (Figure 1.8(c)) is the losing layered geometry of silicate sheets via delamination, where MMT layers are dispersed as nanoscale platelets in the matrix. Exfoliated structure shown in this figure is an idealized

reference morphology rarely seen in practice. Many polymer/MMT nanocomposites including PLA/MMT have mixture of intercalated/exfoliated structure.

There are basically three preparation methods to obtain polymer/MMT nanocomposites: solution mixing, melt mixing and in situ polymerization.

In “solution mixing”; nanoclays are mixed with a solvent having the dissolved chains of the matrix. After removal of the solvent, intercalated and/or exfoliated structure can be obtained.

In “in situ polymerization”; nanoclays are mixed with liquid monomer or monomer solution of the matrix. Then, polymerization occurs in between the intercalated and/or exfoliated clay layers.

In “melt mixing”; polymers and nanoclays are mixed and heated just above the melting point of the polymer used. In this process, polymer chains move into clay galleries and increase the interlayer distance forming intercalated and/or exfoliated structure.

Direct melt intercalation has many advantages over solution intercalation. One of the advantages of melt mixing method is having no solvent molecule diffused into polymer chains which decreases molecular weight of polymer. In addition, the absence of a solvent makes this method an environmentally sound and an economically preferable method [8].

1.4 Weathering Degradation of PLA

Degradation is an irreversible chemical process resulting in undesired changes such as discoloration and loss of mechanical properties limiting the service life of the polymeric components. Apart from the thermal degradation at high temperature

applications, PLA can be also exposed to weathering degradation in outdoor applications.

Polymeric components when used in the atmospheric conditions (i.e. outdoor applications) they are exposed to basically three types of degradation; “photodegradation” due to sunlight, “hydrolytic degradation” due to humidity, and “biodegradation” due to microorganisms in the soil and water. Weathering tests are used to investigate the effects of the first and second one, i.e. the effects of UV irradiation and moisture.

For the PLA structure, the first photodegradation mechanism proposed by Ikada et al. [11] was Norrish type II photocleavage reaction leading to chain scission and the formation of C=C double bonds and carboxylic acid –OH groups at newly formed chains (Figure 1.9).

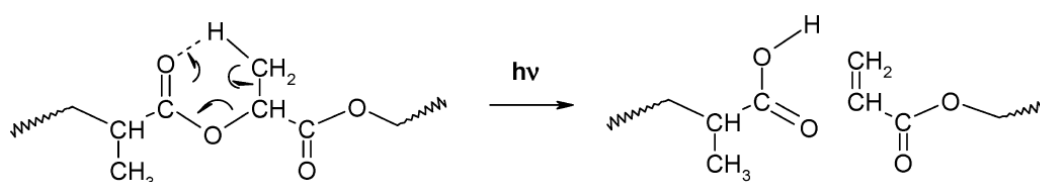


Figure 1.9 Proposed Norrish type II photocleavage reaction for PLA [12].

Later on, Janorkar et al. [13] indicated that photodegradation reaction might proceed with two possibilities, the first one is “photolysis” reaction and the second one is “photooxidation” reaction.

Photolysis mechanism, as shown in Figure 1.10(a), leads to the breakage of the C-O backbone bonds, resulting in decreases in molecular weight.

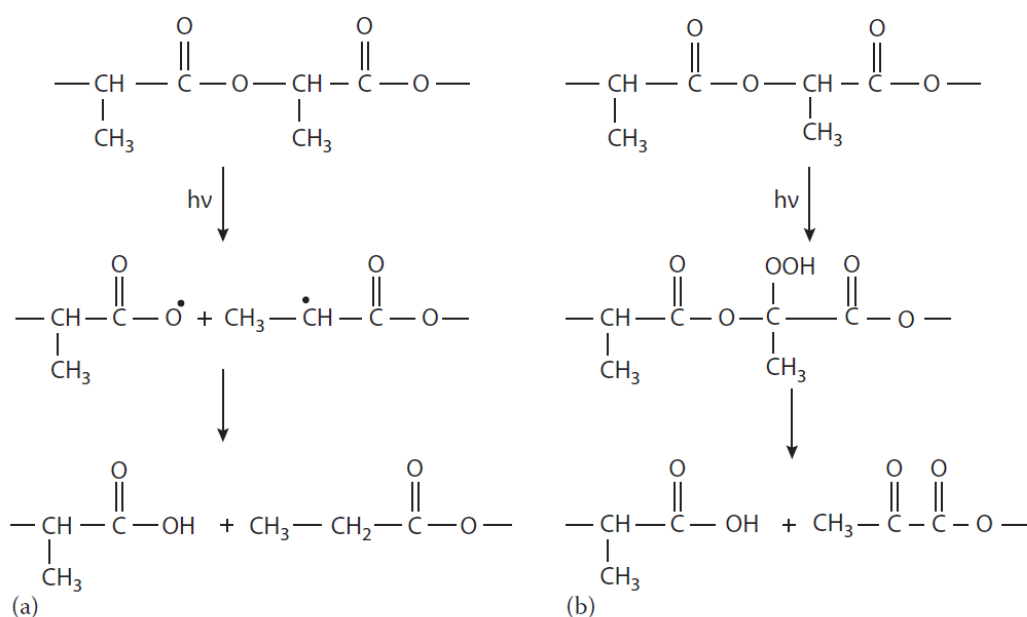


Figure 1.10 Plausible photodegradation mechanisms occurring in PLA. Mechanism (a): photolysis reaction inducing a cleavage of the backbone C–O bond. Mechanism (b): photooxidation of PLA leading to the formation of hydroperoxide derivatives [14].

Photooxidation mechanism, as shown in Figure 1.10(b), leads to the formation of a hydroperoxide derivative and its subsequent degradation to compounds containing a carboxylic acid and diketone end groups. Furthermore, the photolysis of the diketone may lead to the cleavage of C-C bond between the two carbonyl groups, resulting in two carbonyl radicals. This radical pair leads to formation of several photodecomposed products.

Recently, Bocchini et al. [12] also proposed that a series of radical photooxidation reactions could lead to formation of anhydride groups as indicated in Figure 1.11. Photodegradation usually begins by radical formed from impurities by UV light or thermal decomposition. The reaction with higher probability is the abstraction of tertiary hydrogen from PLA chain with the formation of a tertiary radical P• (1). This

radical can react with oxygen and forms a peroxide radical (2). It may easily abstract another hydrogen from a tertiary carbon with the formation of a hydroperoxide and the initial radical $P\cdot$ (3). Then, the hydroperoxide undergoes photolysis (4) with the formation of the $HO\cdot$ and a $PO\cdot$ radical that can further evolve by β -scission (5). Due to the stability of the different fragments, the most probable β -scission appears to be the (5b) reaction, leading to the formation of anhydride groups [12].

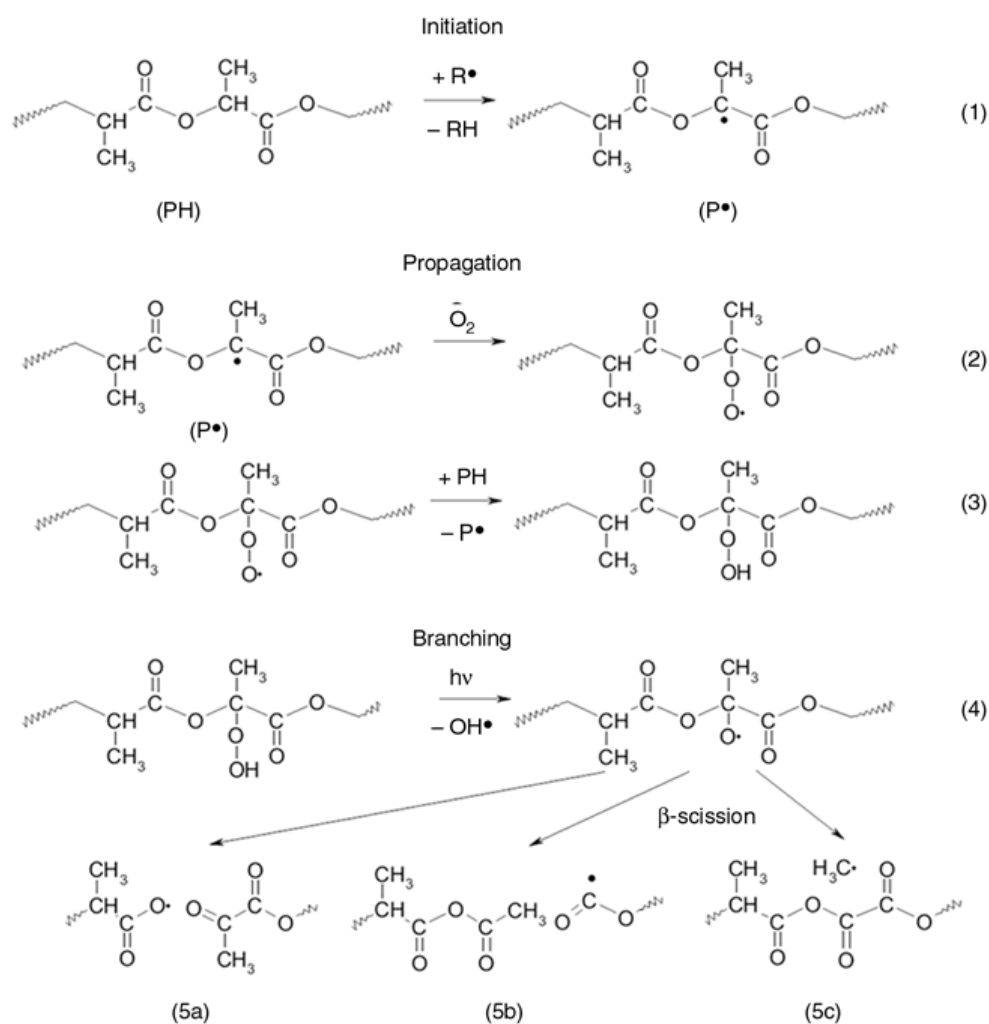


Figure 1.11 Radical oxidation process of UV irradiated PLA samples: Hydroperoxide chain propagation and formation of anhydrides by photolysis of hydroperoxide [12].

In the PLA structure, moisture leads to plasticization and swelling. However, above 30C°, detrimental hydrolytic degradation becomes significant. This degradation mechanism is defined as “hydrolysis”. As shown in Figure 1.12, hydrolysis of PLA backbone occurs through its ester bond. In this reaction, formation of lactic acid oligomers from chain scission lead to higher amount of carboxylic acid end groups and further catalyze the degradation reaction [15, 16].

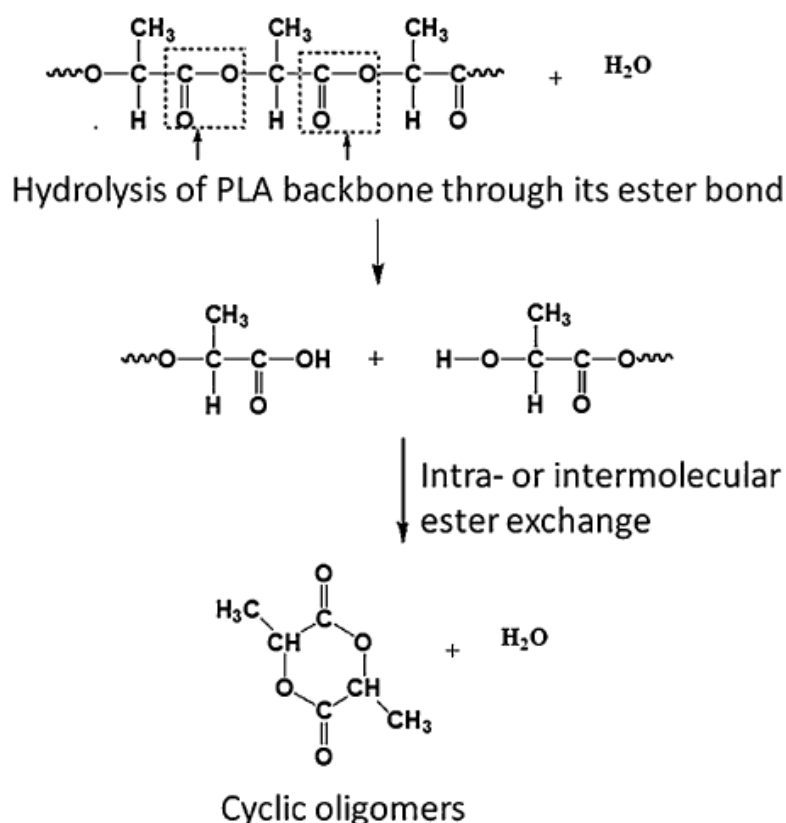


Figure 1.12 Possible hydrolysis reaction of PLA [11].

During weathering, crystallinity amount of PLA might increase due to two reasons. One reason is that, UV irradiation and outdoor temperature might reach to the cold crystallization start temperature of PLA, which is around 70C°. Another reason could be much higher mobility of the short chains of PLA occurred due to chain scissions. This crystallization mechanism is named as “cleavage-induced” crystallization.

1.5 Literature Survey

1.5.1 Previous Studies on the Behavior of PLA/MMT Nanocomposites

Aliphatic biopolyesters, especially poly(L-lactic acid), also called as polylactide (PLA) occupies a predominant area as eco-friendly material in academia and industry due to its biocompatibility and biodegradability in contrast to conventional polymers [17]. Even though PLA has a wide application area in food packaging and biomedical items [18], it also holds a promising future in engineering applications such as automotive components. Therefore, PLA is a sustainable alternative material to petrochemical-derived polymeric materials.

Despite all these advantages, PLA requires higher mechanical and thermal properties to be used in engineering applications. For this purpose, use of “composite approach” is on the rise, i.e. reinforcing the structure of PLA by various inorganic and/or organic fillers. In this respect, one of the most widely used reinforcement is layered silicate nanoclay structures, especially organically modified montmorillonite (MMT) [19]. These materials are named as PLA/MMT nanocomposites.

In the literature, PLA/MMT nanocomposites are investigated basically in two groups. In the first group [20, 21], nanocomposites are produced as “film specimens” usually by “solution intercalation” technique. These specimens were evaluated generally according to their barrier properties.

In the second group [22-29] of the studies, nanocomposites are produced as “bulk specimens” using usually “melt intercalation” technique. These specimens were evaluated generally in terms of mechanical or thermal properties. However, their matrices are not PLA alone, generally blends of PLA with certain elastomeric

materials or other thermoplastics. There seems to be very limited number of studies [30-32] investigating the effects of MMT on the properties of bulk specimens having PLA matrix without reinforcement.

For instance, Jiang et al. [30] indicated that use of 2.5 wt% MMT could increase % elongation at break and toughness of brittle PLA. Beyond that amount, these properties decreased.

Zou et al. [31] reported that use of pristine MMT and organically modified MMT increased crystallinity of PLA from 27 to 33%, and consequently increased the tensile strength and tensile modulus as 17% and 95%, respectively; but the % elongation at break decreased.

Similarly, Ray et al. [32] found that using 4 wt% organically modified MMT could increase flexural strength as 19%, flexural modulus as 12%, and the heat deflection temperature (HDT) from 76 to 91°C.

1.5.2 Previous Studies on the Interfacial Compatibilization of the PLA/MMT Nanocomposites

Apart from organic modification of the silicate layers for efficient intercalation purposes, another modification to improve properties of PLA/MMT nanocomposites further could be the use of maleic anhydride (MA) type modification techniques. In the literature, MA based modifications were conducted generally by the incorporation of maleated elastomeric materials.

For instance, Sabet et al. [33] used MA grafted polypropylene (PP-g-MA), Leu et al. [34] studied maleated styrene-ethylene/butylene-styrene (SEBS-g-MAH), Cumkur et al. [35] investigated ethylene-butyl acrylate-maleic anhydride (E-BA-MA), Mohapatra

et al. [36] used MA with poly(butylene adipate-co-terephthalate) (PBAT), and Pluta et al. [37] added a MA functionalized elastomeric ethylene copolymer. These studies [33-37] basically indicated that due to the elastomeric nature of their maleated modifiers, ductility and toughness of PLA/MMT nanocomposites were improved.

However, to the best of our knowledge, there is only one study [38] using MA grafted PLA copolymer (PLA-g-MA) as the compatibilizer. In this study, Jiang et al. [38] used PLA-g-MA for the MMT reinforced matrix of not PLA alone, but a blend of PLA/PBAT. They revealed that the ternary composite composition PLA/10 wt% PBAT/2.5 wt% MMT with PLA-g-MA obtained the highest mechanical properties.

1.5.3 Previous Studies on the Accelerated Weathering Behavior of PLA and its Composites

PLA is a biodegradable biopolymer having aliphatic polyester structure with thermoplastic character. It has found wide range application area in food packaging and biomedical items and increasing commercial interest due to its desired mechanical strength, thermal stability and biocompatibility. PLA is also the center of interest with being an alternative to petroleum-based polymers, because PLA is synthesized from agricultural renewable resources.

One of the drawbacks of PLA is its sensitivity to atmospheric conditions, i.e. UV irradiation, moisture and temperature. When viewed from this aspect, PLA with the enhanced outdoor performance is essential in many engineering applications such as automotive parts. Therefore, its weathering performance should be determined either naturally or artificially. In natural weathering, sun is the UV irradiation and temperature source while rain and atmospheric humidity are the source of moisture.

Testing of polymeric materials under “natural weathering” conditions strongly depends on the chosen site and chosen exposure time which are usually very long periods such as 1-5 years. On the other hand, “artificial weathering” conditions are reproducible by applying constant or cyclic exposure of certain levels of UV irradiation, temperature and moisture via an electronic control unit such as “accelerated weathering tester” systems. Since, a correlation can be established between natural and artificial weathering, use of accelerated weathering tester systems are very practical and quick compared to the time consuming natural weathering.

Until recently, biodegradation of PLA based materials have been clarified by many researchers, but less study has been performed on the weathering performance (hydrolytic degradation and/or photodegradation) of neat PLA [12, 15 39-44], and the PLA composites with inorganic fillers such as talc [45], calcium sulfate [46, 47,], silica [48], carbon nanotube [49] and titanium dioxide [50, 51].

Some of the studies [40, 46] indicated that photodegradation of PLA proceed via the Norrish II type photocleavage reaction leads to random chain scission (decrease of molecular weight), and the formation of C=C double bonds and hydroperoxide O-H at newly formed chains. Some of them [15, 39, 47, 50-52] further indicated that UV irradiation leading to random main chain scission in certain chemical bonds of the PLA structure occurs via “photolysis” and/or “photooxidation” mechanisms leading to formation of carboxylic acid and diketone groups. Later on, Bocchini et al. [12] proposed that photooxidation could also lead to formation of anhydride groups.

Another group of these studies [41-45, 47] revealed that hydrolytic degradation of PLA due to the moisture mainly proceed via “hydrolysis” mechanism; that is cleavage of the ester bonds in the PLA backbone leading to again successive chain scission with reduced molecular weight.

In the literature, there are also certain number of studies investigating the weathering performance of PLA composites reinforced with certain clay minerals such as bentonite [52], semectite [53], halloysite [54] and the most attractive one montmorillonite (MMT) [55-63]. Some of these PLA/MMT studies investigated effects of photodegradation either under artificial UV lamb irradiation [12, 55, 56] or under natural outdoor sunlight [57]; some of them revealed effects of hydrolytic degradation either in certain solutions [58-60] or under ambient humidity for very long periods [57, 61-63]. In some of these MMT nanocomposites matrix was not neat PLA, but it was blends of PLA, such as with linear low density polyethylene (LLDPE) [58], poly(ethylene oxide) (PEO) [61] and poly(ethylene glycol) (PEG) [62, 63]. Unfortunately, none of these studies conducted accelerated weathering tests of both UV irradiation and moisture.

Literature survey indicated that there is only one recent study investigating the artificial weathering (both UV and moisture) of PLA/MMT nanocomposites. In this study, Chavez-Montes et al. [64] compared accelerated weathering performance of MMT nanocomposites having amorphous and semicrystalline PLA matrices. Their comparison was based on the decrease of the molecular weight of PLA. They reveal that weathering degradation was favored more in the amorphous matrix compared to semicrystalline PLA matrix. That work also includes a correlation between natural and artificial weathering, but no comparison in the changes of mechanical or thermal properties.

1.6 Purpose of the Study

In order to contribute to very limited number of PLA/MMT studies discussed in the Section 1.5.1, the main purpose of the first part of this thesis is to investigate effects of organically modified MMT content on the significant engineering properties of PLA, i.e. strength and modulus under flexural and tensile loading; including ductility

and fracture toughness. Moreover, all PLA/MMT nanocomposites were produced by industrially compatible production techniques, i.e. twin-screw extrusion melt-mixing for compounding and injection molding for shaping of bulk specimens.

Another missing point in the literature is the interfacial studies of PLA/MMT nanocomposites. To the best of our knowledge, there is only one study using MA compatibilization, but in this study the matrix is not PLA alone, it is a blend of PLA/PBAT. Thus, another purpose of the first part of this thesis is, as the first time, to investigate the influences of PLA-g-MA copolymer compatibilization on the engineering mechanical properties of MMT nanocomposites having the matrix of PLA alone.

As indicated in Section 1.5.3, there is only one PLA/MMT study investigating effects of artificial weathering on the decrease of the molecular weight of amorphous and semicrystalline PLA. But, in this work no comparison in the changes of mechanical or thermal properties were made. Therefore, as the first of its kind, the purpose of the second part of this thesis is to determine accelerated weathering (both UV and moisture) performance of neat PLA and its 1 wt% MMT nanocomposite by comparing their mechanical properties and thermal behavior at four different weathering periods.

CHAPTER 2

EXPERIMENTAL WORK

2.1 Materials Used

In the thesis, commercial L-lactic acid type polylactide (PLA) supplied by NaturePlast (France) with an extrusion grade (PLE 001) was used as the matrix material. According to its technical data sheet, it has a melting temperature range of 145-155°C, degradation temperature range of 240-250°C, while the melt flow index range at 190°C under 2.16 kg is 2-8 g/10 min, as well as a density of 1.25 g/cm³. Moreover, weight average molecular weight of this PLA was determined using the static light scattering (SLS) spectroscopy technique via Malvern CGS-3 giving the result of 375 600 g/mol.

The montmorillonite (MMT) type nanoclay used was Cloisite 30B obtained from Southern Clay Products (Gonzalez, USA). Cloisite 30B was organically modified with methyltallow bis-2-hydroxyethyl quaternary ammonium cation (MT2EtOH). The particle size range of the nanoclay was 2–13 µm.

Maleic anhydride (MA) (Sigma-Aldrich, purity 99%) used for grafting of PLA has molecular weight of 98.06 g/mol, melting temperature range of 51-56°C and boiling temperature of 200°C. Initiator used for MA grafting reaction was dicumyl peroxide (DCP) (Sigma-Aldrich, purity 99%) with melting temperature of 39°C.

2.2 Production of PLA/MMT Nanocomposites

PLA/MMT nanocomposites were produced by two industrially compatible steps; i.e. “twin-screw extrusion melt-compounding” and “injection molding melt-shaping” with laboratory size equipment.

In the first step, PLA granules and MMT powders were pre-dried for 15 hours in a vacuum oven at 60°C, and then pre-mixed manually. This mixture was melt compounded via Rondol Microlab 300 laboratory size (D=10 and L/D=20) twin-screw extruder. Typical temperature profile from feeder to die used were 115°-170°-180°-175°-150°C while the typical screw speed used was 70 rpm throughout the compounding stage; followed by four-blade cutting of the continuous strands into pellets of 2-3 mm.

In the second step, prior to shaping, pellets were again allowed to re-dry for 15 hours in a vacuum oven at 60°C. Standard sized specimens required for testing and analyses were melt-shaped via a laboratory scale DSM Xplore Micro injection molder. Typical barrel and mold temperatures used were 185°C and 35°C, respectively; while the melting time in the barrel was approximately 7 minutes, with the subsequent three-step pressure-time profile determined as 14 bar for 3 s, 12 bar for 5 s, and 12 bar for 5 s.

PLA nanocomposites were produced with the loadings of 0.5, 1, 2 and 3 wt% MMT. These nanocomposites were designated using the format of “PLA/MMT x ”, where x denotes wt% of MMT used.

2.3 Production of PLA/gMA/MMT Nanocomposite

MA based compatibilization was applied only for the PLA/MMT 1 nanocomposite composition; because, as will be discussed in Results and Discussions chapter, addition of 1 wt% MMT resulted in optimum mechanical properties.

Effects of interfacial compatibilization was conducted using the MA grafted PLA copolymer, i.e. PLA-g-MA. For this purpose, different amounts of the copolymer was compounded with the PLA/MMT 1 composition, and it was revealed that use of 3 wt% PLA-g-MA copolymer resulted in optimum properties. Thus, only this composition was evaluated. For simplicity, PLA-g-MA copolymer was designated as “gMA” in this study. Therefore, that specimen having MA based compatibilization was designated as “PLA/gMA/MMT 1”.

Note that PLA-g-MA copolymer was produced using the reactive extrusion technique via twin-screw melt mixing of PLA and 2 wt% MA including 0.5 wt% dicumyl peroxide (DCP) as the free radical initiator. By using the titration method, the amount of grafted MA on PLA was found as 1.18%. Details of these procedures are explained in our former study [65] thoroughly.

2.4 Structural Characterization by XRD, TEM, FTIR and SEM

Formation of PLA/MMT nanocomposite structure was first determined by X-ray diffraction (XRD) analysis with Bruker D8 Advance A25, CuK α radiation, 40 kV, 40 mA, over a scanning range of 1 $^{\circ}$ -10 $^{\circ}$.

Then, in order to evaluate dispersion and level of intercalation/exfoliation of MMT silicate layers in PLA matrix, transmission electron microscopy (TEM) was conducted with FEI Tecnai G2 Spirit Bio TWIN at an acceleration voltage of 80 kV. Samples

were prepared under a Leica EM UC6 ultra-microtome with diamond knife. Around 100 nm thick sections sliced were transferred onto copper grids of 400 mesh.

In order to reveal possible interfacial interactions between PLA, MA and MMT fillers, “Fourier transform-infrared (FTIR) spectroscopy” was used. At least 32 scans were signal-averaged by the “attenuated total reflectance (ATR)” unit of Bruker ALPHA IR spectrometer in the wavenumber range of 400 to 4000 cm^{-1} with a resolution of 4 cm^{-1} .

Fracture surface morphology of the fracture toughness specimens were carried out for the gold sputtered surfaces using a FEI Nova Nano 430 scanning electron microscope (SEM).

2.5 Mechanical Tests and Thermal Analyses

K_{IC} and G_{IC} fracture toughness tests were conducted for single-edge-notched-bending specimens according to ISO 13586 standard under Instron 5565A system. Notches and pre-cracks on these specimens were created by Ceast Notchvis system as defined in the standard. Apart from toughness tests; tension and flexural tests were also carried out to determine other mechanical properties of the specimens. Tension tests were applied according to ISO 527-2 standard, while flexural tests in terms of three-point bending were applied according to ISO 178 standard. These tests were carried out using a 5 kN Instron 5565A universal testing system. For each specimen group, these tests were repeated 5 times; and mechanical properties were determined as the average values including their standard deviations.

The first thermal analysis to determine transition temperatures and enthalpies of each specimen was differential scanning calorimetry (DSC) analyses. The heating profile used for the materials was from -80° to 220°C with $10^{\circ}\text{C}/\text{min}$ rate using a SII X-DSC

700 Exstar system. The second analysis for the determination of the thermal degradation temperatures of each specimen was through thermogravimetric analyses (TGA). This time the heating profile was from 30° to 550°C via a SII TG/DTA 7300 Exstar system.

2.6 Accelerated Weathering of the Neat PLA and its PLA/MMT Nanocomposite

As discussed in the “Results and Discussion” chapter of this thesis, it was revealed that use of 1 wt% MMT resulted in the best optimum mechanical properties. Therefore, in the second part of this thesis, influences of accelerated weathering were explored for the PLA/MMT nanocomposites having only 1 wt% MMT.

In order to investigate the weathering behavior of neat PLA and its 1 wt% MMT nanocomposite, an *accelerated weathering tester* (Q-LAB Model QUV/se) was used. The weathering conditions were in accordance with the Cycle-C of the SAE J2020, ASTM G154-05 and ISO 4892-3 standards. Fluorescent lamps (UVB-313) with 0.49 W/m² irradiance (at 310 nm) were used with cycles of 8 h UV irradiation at 70°C, followed by 4 h dark condensation at 50°C. These consecutive cycles were applied to the specimens attached to the test panels without any interruption. Effects of accelerated weathering were investigated for four periods: 50, 100, 150 and 200 h. Specimens for each period were designated as PLA/MMT-*x*h, where *x* denotes the accelerated weathering period.

Effects of each period of accelerated weathering on the behavior of the neat PLA and its 1 wt% MMT nanocomposite specimens were investigated by comparing the changes in the results of the following tests and analyses conducted.

2.7 Changes in the MMT Intercalation and PLA Crystallinity

The same XRD equipment mentioned before was also used to reveal the effects of each accelerated weathering period on the variation in the intercalated structure of MMT layers and also crystallinity of the neat PLA plus matrix of 1 wt% MMT nanocomposite specimens. For the determination of intercalated structure, 2θ diffraction angle scanning was from 1° to 8° , while for the matrix crystallinity from 5° to 25° , respectively.

2.8 Changes in the Color of the Specimens

Variation in the color of the specimens after each accelerated weathering period was observed both visually and quantitatively. Visual observation was done by photographing the images of the weathered specimens and comparing their color with the unweathered one.

The quantitative analysis for the color change was conducted by determining the CIELAB color space parameters (L^* , a^* , b^*) of the specimens before and after each accelerated weathering period. For this purpose *diffused reflectance analysis* (DRA) was utilized via DRA unit of Agilent Cary 60 UV-vis spectrophotometer in accordance with CIE 1976 standards.

2.9 Changes in the Chemical Structure of the Specimens

For the variation in the chemical structure of the specimens, the first analysis was to observe the decreases in the molecular weight of PLA matrix after each accelerated weathering period. For this purpose, *static light scattering* (SLS) spectrometry

(Malvern CGS-3) was conducted to determine the weight-average molecular weight (M_w) of the specimens using the results of Guiner plots of four different concentrations of PLA samples dissolved in chloroform.

The second analysis was *attenuated total reflectance-Fourier transform infrared spectroscopy* (ATR-FTIR) to observe the changes in the chemical bonds of the specimens after each accelerated weathering period. Spectra were taken via ATR unit of Bruker ALPHA with signal-averaged 32 scans at a resolution of 4 cm^{-1} within the wavenumber range of 400 to 4000 cm^{-1} .

2.10 Changes in the Fracture Surface Morphology, Mechanical Properties and Thermal Behavior of Specimens

In order to compare changes in the fracture surface morphology, tensile and flexural modulus, tensile and flexural strength, ductility, fracture toughness, transition and thermal degradation temperatures of the neat PLA and its 1 wt% MMT nanocomposite specimens before and after each accelerated weathering period, SEM observations, mechanical tests and thermal analyses mentioned in the above Sections 2.4 and 2.5 were performed.

CHAPTER 3

RESULTS AND DISCUSSION

As stated before, since this dissertation has two different parts, their results are presented and discussed successively in the following two subsections.

3.1 Effects of MMT Content and MA Compatibilization

3.1.1 Intercalated Structure of the PLA/MMT Nanocomposites

It is known that mechanical properties of the polymer matrices could be improved if uniformly distributed silicate layers of MMT have certain level of intercalation and/or exfoliation; i.e. entrance of the macromolecular chains of PLA into the galleries in between the MMT layers.

One of the best way to quantify the extent of intercalation is the comparison of the XRD patterns of the MMT with the patterns of the nanocomposites. Figure 3.1 shows that organically modified MMT (Cloisite 30B) gives very sharp (001) reflection at $2\theta=4.9^\circ$. According to the Bragg's equation, this reflection results in an interlayer distance (d_{001}) of 1.8 nm. Figure 3.1 also shows that diffraction peak of the PLA/MMT nanocomposites shifts to around 1.84° ; this time Bragg's relation gives an increased d_{001} gallery distance of around 4.79 nm. That is, MMT layers were intercalated by the macromolecular chains of PLA.

It was also observed that there was no significant difference in the positions of the diffraction peak of each PLA/MMT nanocomposite. Compared to the sharp and high

intensity peak of organically modified MMT, it is seen in Figure 3.1 that reflection peaks of the PLA/MMT nanocomposites have low intensity. This could be interpreted as having not only “intercalation”, but also certain level of “exfoliation” of the MMT silicate layers in the PLA matrix.

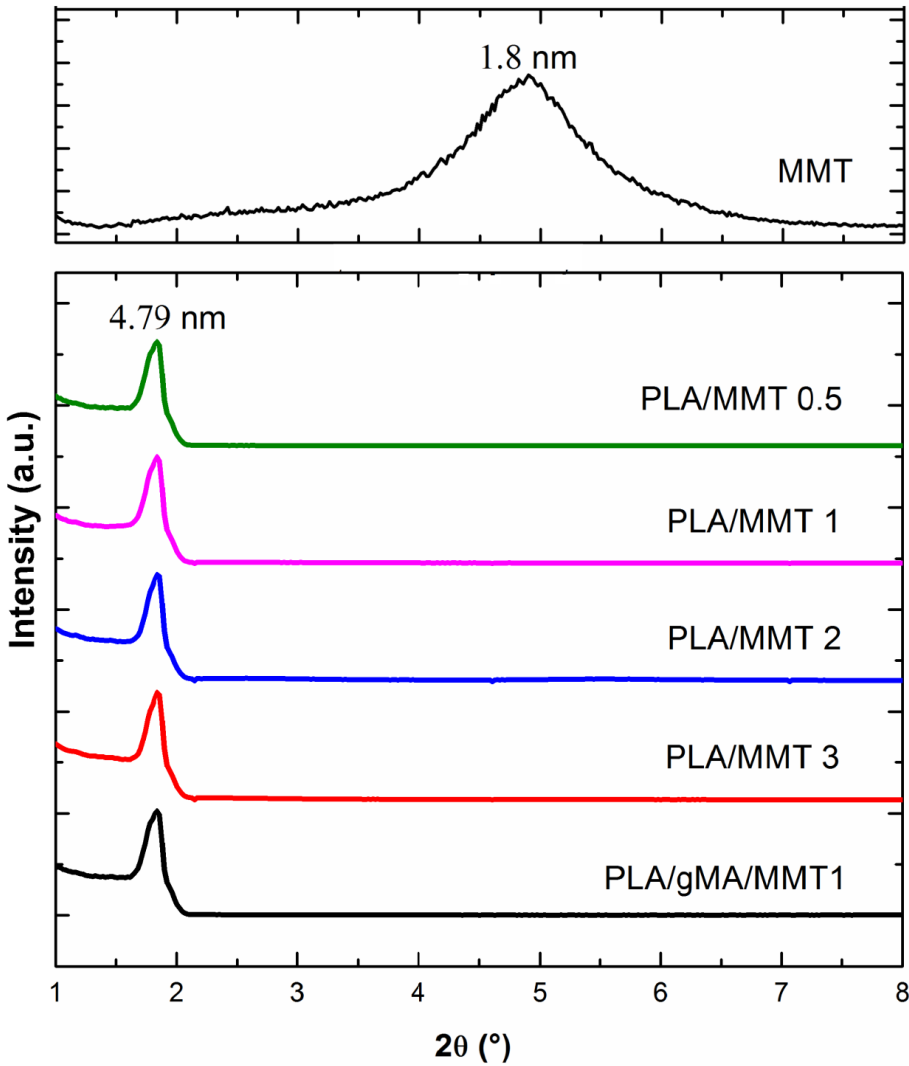


Figure 3.1 XRD Patterns of the organically modified MMT and PLA/MMT Nanocomposites.

In order to support XRD results visually, PLA/MMT nanocomposites were also examined by TEM analysis. Images in Figure 3.2(a) and (b) with low magnification show that distribution of MMTs in the PLA matrix was rather uniform and homogeneous; while images in Figure 3.2(c) and (d) with high magnification reveal that MMT layers have certain level of intercalation and exfoliation.

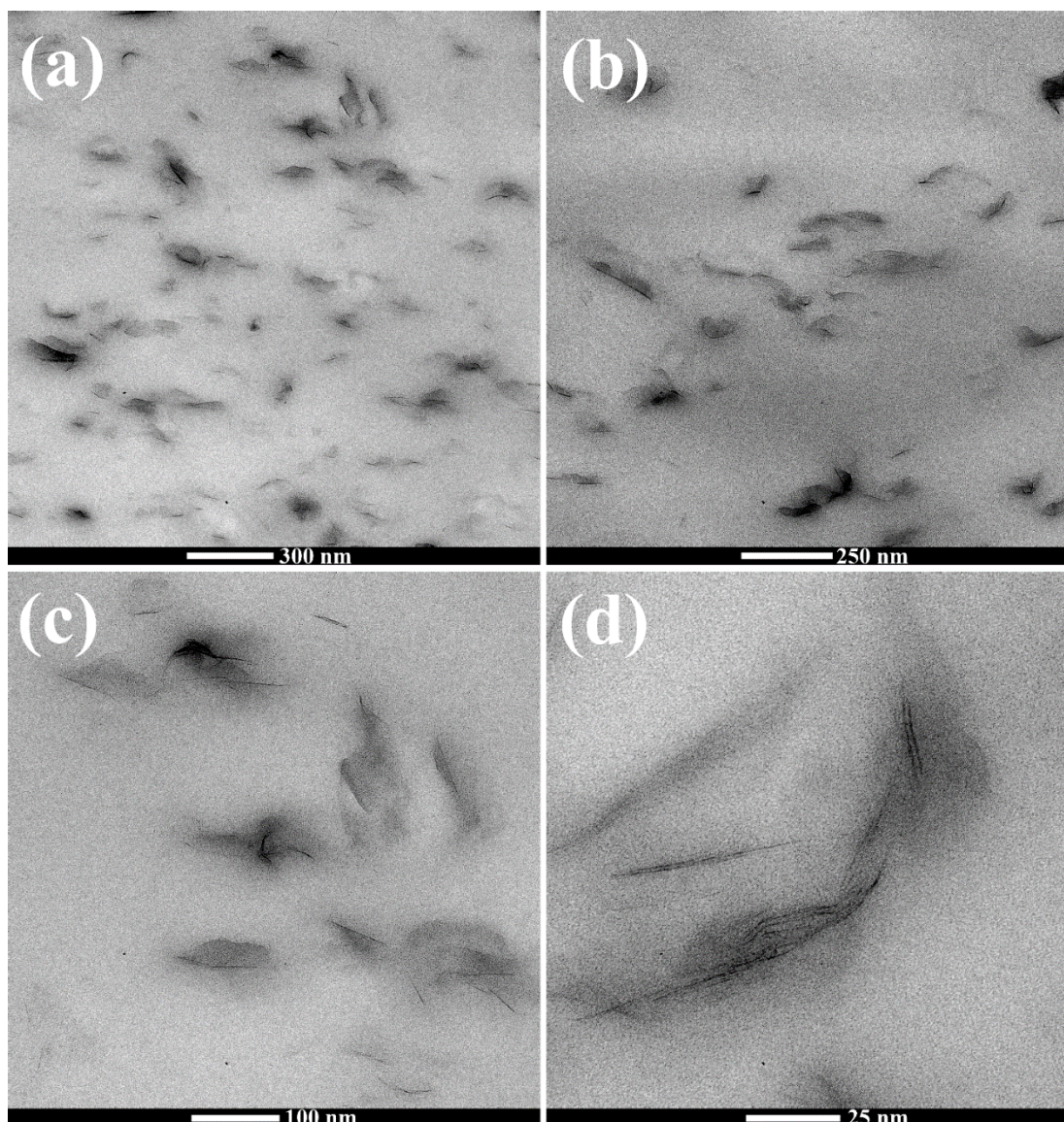


Figure 3.2 TEM Images Showing (a) and (b) Uniform Distribution, (c) and (d) Intercalation/Exfoliation of MMT Layers in PLA matrix.

3.1.2 Chemical Structure of PLA/MMT Nanocomposites

Chemical structure of the specimens was evaluated by comparing the ATR-FTIR spectra (Figure 3.3) of the neat PLA and PLA/MMT nanocomposites with and without MA compatibilization. Figure 3.3 first shows IR spectrum of the neat PLA specimen used in this study having mainly five regions: the C-C stretching at 867 cm^{-1} , the C-O stretching peaks at $1079, 1126, 1181, 1264\text{ cm}^{-1}$, the C-H deformation peaks at $1377, 1452\text{ cm}^{-1}$, C=O ester carbonyl groups at 1748 cm^{-1} , and the C-H stretching at $2853, 2924\text{ cm}^{-1}$. These characteristic IR band assignments observed are all in accordance with the ones discussed in the literature [66-68].

It is known that when there is no chemical interaction between the polymer matrix and the reinforcement in composite materials; then there would be no changes in the IR spectra of the polymer matrix material. However, when there is a certain level of interaction such as hydrogen bonding or dipolar interaction between the polymer matrix and the reinforcement; then there would be some changes in the IR spectrum of the composite, usually in the form of band shifting and broadening.

It has been discussed that [69] when MMT was incorporated into PLA matrix, typical IR bands of the silicate layers could appear, such as Al-O stretching at around 520 cm^{-1} and Si-O bonding at around 627 cm^{-1} . These tiny peaks can be seen in the spectrum of PLA/MMT 1 specimen in Figure 3.3.

Moreover, it was indicated by Jiang et al. [30] that there could be interaction between the hydroxyl end groups of PLA and the hydroxyl groups present on the surfaces of MMT layers plus in the structure of the organic modifier. This interaction generally appears as the shift of the C-O stretching of PLA and/or O-H stretching of the end groups of PLA to lower wavenumbers. In the present study as seen in the spectrum of PLA/MMT 1 specimen in Figure 3.3; the C-O stretching peaks of PLA at $1079, 1126,$

1181, 1264 cm^{-1} , all shifted to the lower wavenumbers of 1027, 1094, 1164, and 1257 cm^{-1} , respectively.

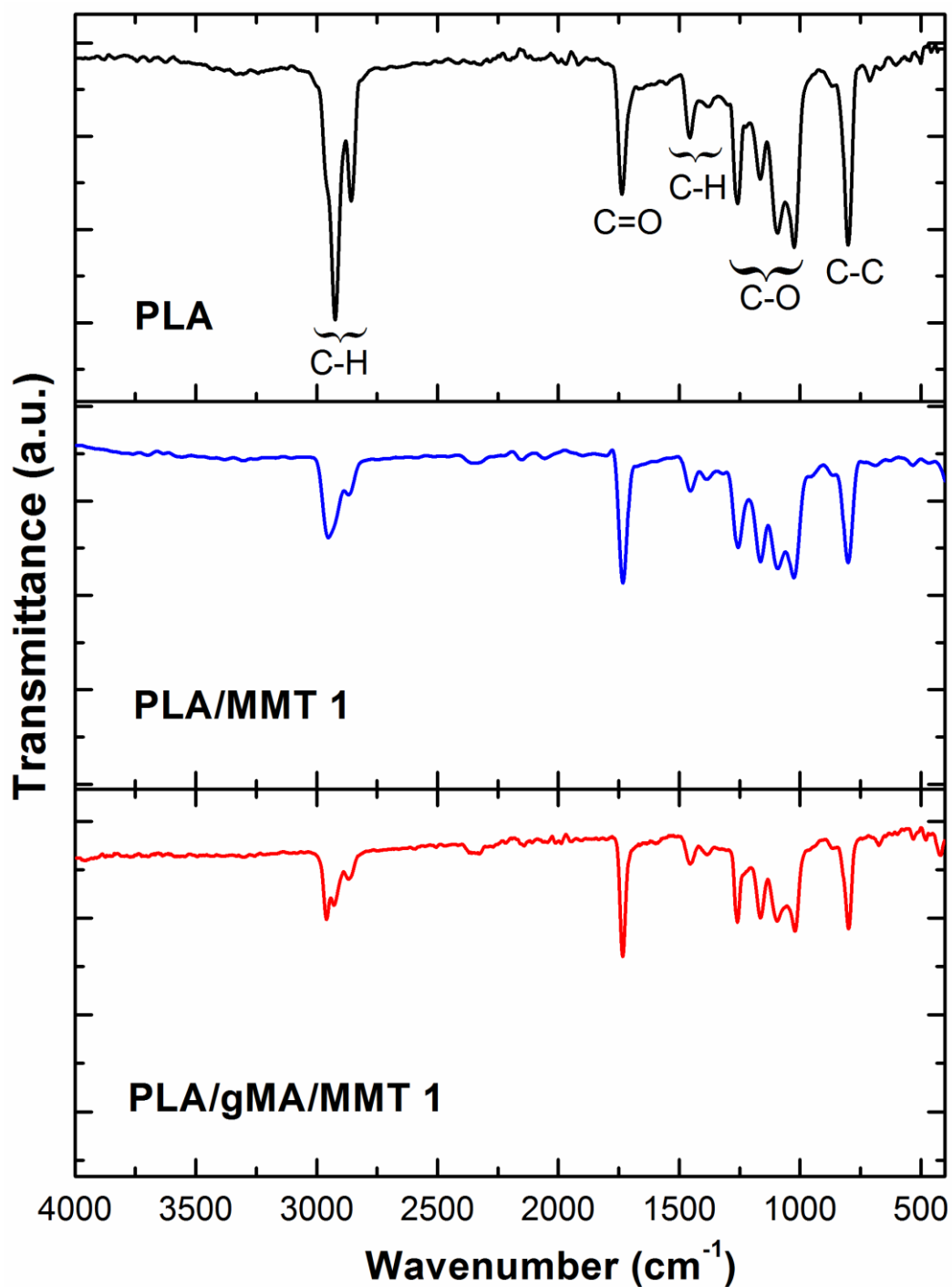


Figure 3.3 ATR-FTIR spectra of neat PLA and PLA/MMT nanocomposites.

In the literature [70], typical IR assignments discussed for the MA structure are cyclic C=C stretching band at 1590 cm^{-1} , asymmetric and symmetric C=O stretching at 1774 cm^{-1} and 1850 cm^{-1} , respectively. After MA compatibilization via use of MA grafted copolymers, the expected interaction was between the oxygen of the carbonyl groups of MA and the hydrogen of the hydroxyl groups present in the structure of the polymer matrix, and/or on the surfaces of MMT layers, and/or in the structure of the organic modifier of the MMT.

As stated in the literature [35, 71] that kind of interaction could be observed mainly by shifting or decreased intensity of the C=O of MA at around 1774 cm^{-1} ; or disappearance of this peak due to the conversion of the maleic anhydride groups into maleic acid groups. In this case, carbonyl groups would change to hydroxyl groups, resulting in the appearance of new O-H stretching peaks at around 3620 cm^{-1} . On the other hand, as seen in Figure 3.3, C=O peak of MA was overlapped by the C=O peak of PLA, preventing the possible interpretations to make.

3.1.3 Modulus and Strength of the PLA/MMT Nanocomposites

Effects of MMT content and MA compatibilization on the modulus and strength of PLA was investigated by first three-point bending and then tension tests. Figure 3.4 gives “flexural stress-strain” curves and “tensile stress-strain” curves of the specimens separately, while Table 3.1 tabulates values of “Flexural and Tensile Modulus (E_{Flex} and E)” and “Flexural and Tensile Strength (σ_{Flex} and σ_{TS})” determined by these tests. Furthermore, influences of different amount of MMT and MA compatibilization on these modulus and strength values of the nanocomposites are also evaluated in Figures 3.5. Note that the data for the PLA/gMA/MMT 1 specimen in the x -axes of Figure 3.5 was designated as “gMA” for simplicity.

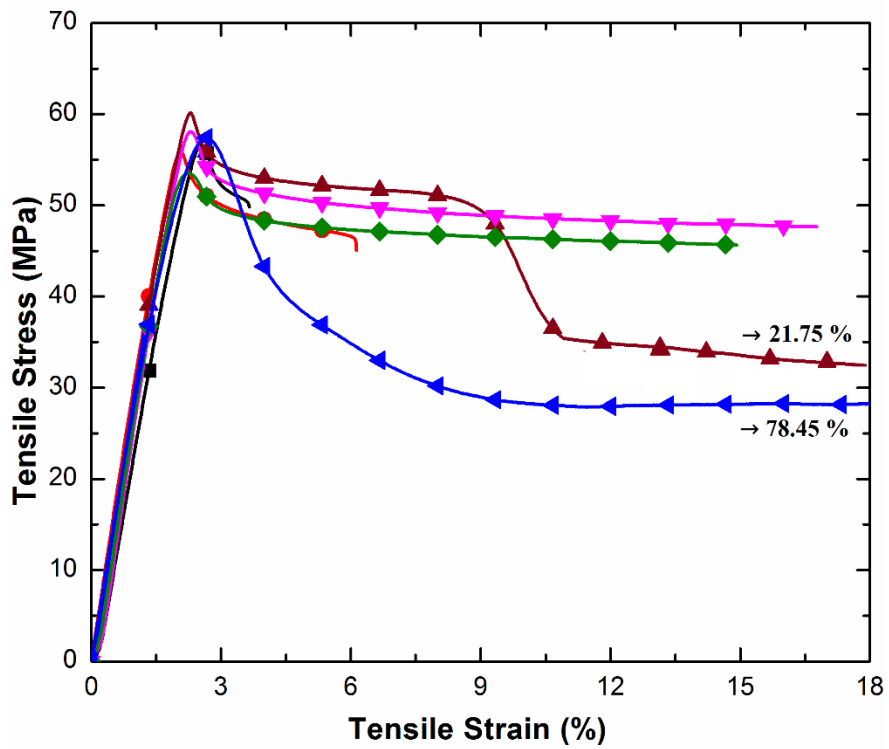
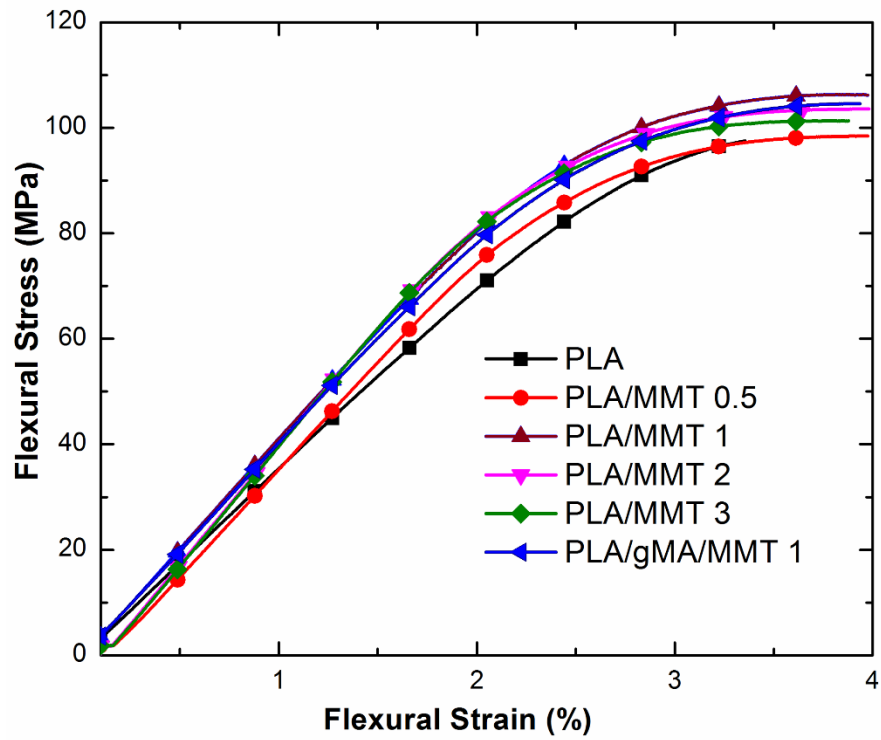


Figure 3.4 Stress-strain curves of the specimens obtained during three point bending flexural and tensile tests.

It is known that when a rigid and strong filler is added into a matrix of polymeric material, the mobility of its macromolecular chain structure decreases. The basic influence of that decrease is in the stiffness of the polymers, i.e. improved elastic modulus values. Table 3.1 and Figure 3.5 show that incorporation of MMT increases flexural and tensile modulus values of PLA successively, due to the decreased mobility of the PLA chains by the intercalated/exfoliated MMT layers. Table 3.1 indicates that the highest improvement in modulus values were obtained by the use of 2 wt% MMT; leading to 27% increase in E_{Flex} and 15% increase in E values, respectively.

Table 3.1 Flexural modulus (E_{Flex}), tensile modulus (E), flexural strength (σ_{Flex}) and tensile strength (σ_{TS}) values of the specimens

Specimens	E_{Flex} (GPa)	E (GPa)	σ_{Flex} (MPa)	σ_{TS} (MPa)
PLA	3.60±0.07	2.85±0.08	97.9±1.3	58.6±1.4
PLA/MMT 0.5	4.04±0.01	3.07±0.07	99.9±3.9	59.6±1.6
PLA/ MMT 1	4.18±0.09	3.17±0.08	104.2±1.3	61.0±0.6
PLA/ MMT 2	4.57±0.06	3.28±0.06	102.5±1.9	57.8±0.5
PLA/ MMT 3	4.56±0.06	3.24±0.10	101.1±0.4	55.8±1.5
PLA/gMA/ MMT 1	4.14±0.06	3.01±0.08	103.0±2.2	59.3±2.1

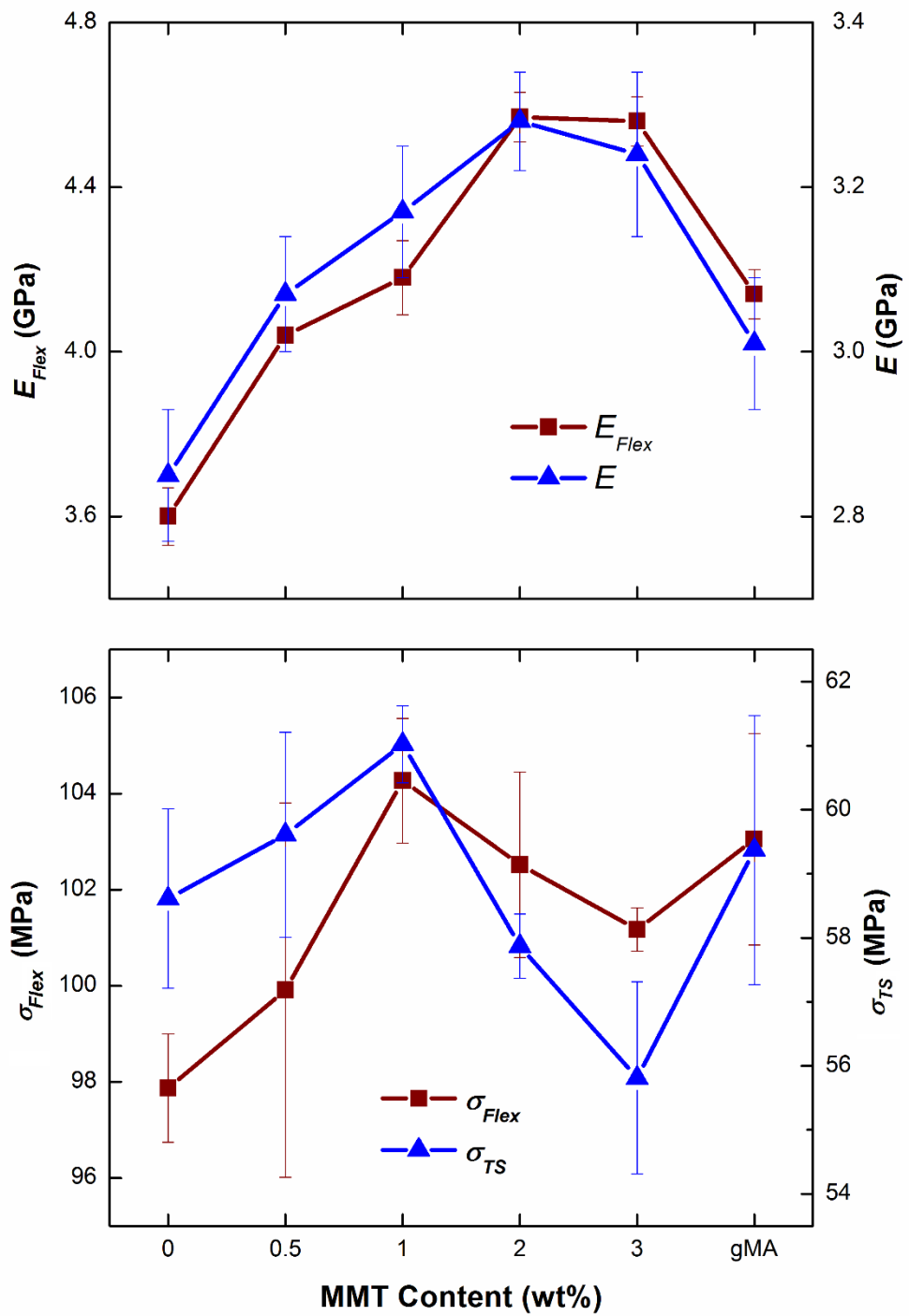


Figure 3.5 Effects of MMT content and MA compatibilization on the modulus and strength of the specimens (note that gMA in the x -axes denotes PLA/gMA/MMT 1 specimen).

Apart from chain mobility decrease, another influence of the incorporation of rigid and strong filler into a polymer matrix will be their load carrying ability. That is, if there is sufficient degree of interfacial attraction between the matrix and filler; then applied loads can be transferred from the weaker polymer matrix to the stronger filler material. Table 3.1 and Figure 3.5 indicate that strength values of PLA increase by the incorporation of MMT, due to the applied stress transfer from the PLA matrix to the intercalated/exfoliated MMT layers having very high nano range aspect ratio.

This time Table 3.1 shows that the highest strength values are obtained using 1 wt% MMT; leading to 7% increase in σ_{Flex} and 4% increase in σ_{TS} values, respectively. Beyond this amount, due to the possibility of MMT agglomeration, strength values started to decrease slightly.

It was also revealed that use of MA compatibilization resulted in no further improvements in the modulus and strength values of the PLA/MMT nanocomposites; these properties remained almost unchanged. On the other hand, as will be discussed in the next section, there were significant improvements in the ductility and toughness values.

3.1.4 Ductility and Toughness of the PLA/MMT Nanocomposites

In tension tests apart from modulus and strength values another measurement is the amount of plastic strain formed until fracture, i.e. “% strain at break”. That measurement is considered as “ductility” of materials which represents the total amount of permanent plastic deformation occurred up to fracture of the specimen. Figure 3.4 shows that tensile stress-strain curve of neat PLA specimen is very linear with very little amount of plastic strain. On the other hand, when MMT particles were added the stress-strain curves become non-linear possessing large amounts of plastic strain.

Ductility of the specimens was also evaluated by comparing the final appearance of their gage length visually as given in Figure 3.6. The images in this figure show that use of MMT and MA compatibilization increase the level of ductility (in terms of final strain at break), significantly.

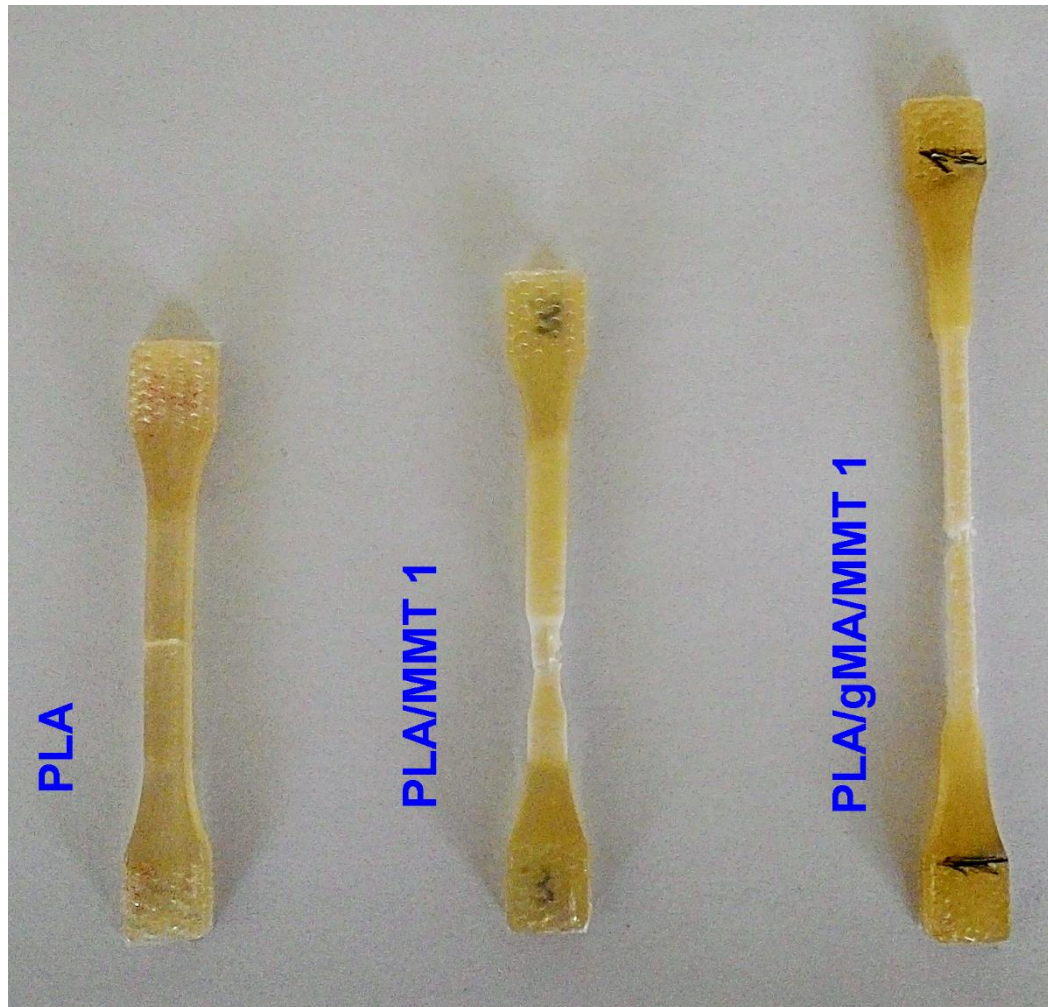


Figure 3.6 Effects of MMT and PLA-g-MA compatibilization on the ductility of the specimens in terms of tensile elongation at break.

It is seen in Figure 3.6 that neat PLA has flat fracture point, having almost no necking, due to its very brittle nature. When MMT was incorporated the gage length increases

significantly until fracture. Around the necked region, certain level of “whitening” is apparent. In this region, the porous structure with load bearing fibrils and the intercalated/exfoliated MMT layers prevent the early fracture; thus higher elongation was possible.

After MA compatibilization, Figure 3.6 indicates that the gage length of the specimen has been elongated enormously almost having no necking with entirely “whitened” structure. That outstanding improvement in ductility can be explained with the improved interaction between the PLA chains and MMT layers via MA compatibilization preventing the earlier fracture under tensile load.

In this study ductility values of the specimens were determined as % final strain at break (ϵ_f) from their tensile stress-strain curves; and tabulated in Table 3.2, and compared according to effects of MMT content and MA compatibilization in Figure 3.7. Table 3.2 and Figure 3.7 show that ductility of all PLA/MMT nanocomposites are much higher than for the neat PLA. The best improvement is again with 1 wt% MMT, increasing the ϵ_f value from 3.48% up to 21.75%, i.e. an increase of more than 6 times. After MA compatibilization, the enormous increase of ductility in terms of ϵ_f becomes 78.45%, i.e. an increase of more than 22 times.

Since the most significant deficiency of the biopolymer PLA is its inherent brittleness, toughness is the key property to be improved for many engineering applications. Therefore, in this research, influences of MMT content and MA compatibilization on the toughness of PLA were studied by “Fracture Toughness” tests. Because, it is one of the most critical parameter required in many structural applications. This test basically measures ability of the materials to resist initiation and propagation of cracks. In this study, fracture toughness tests were evaluated in terms of “Critical Stress Intensity Factor (K_{IC})” and “Critical Strain Energy Release Rate (G_{IC})” values; and tabulated in Table 3.2, and also compared according to effects of MMT content and MA compatibilization in Figure 3.7.

K_{IC} and G_{IC} fracture toughness values given in Table 3.2 and Figure 3.7 reveal that increases were slight with 0.5 wt% MMT, but become very high with the incorporation of 1 wt% MMT. For this specimen, the increases in K_{IC} value is 31%, and in G_{IC} value 85%, respectively. Beyond this MMT content, these values decreased again due to the possibility of MMT agglomeration. Just like ductility values, after MA compatibilization there were further improvements, this time the increases in K_{IC} and G_{IC} values become 70% and 119%, respectively.

Table 3.2 Tensile Strain at Break (ϵ_f) and Fracture Toughness (K_{IC} and G_{IC}) Values of the Specimens

Specimens	ϵ_f (%)	K_{IC} (MPa \sqrt{m})	G_{IC} (kJ/m ²)
PLA	3.48 ± 0.25	3.43±0.04	5.44±0.34
PLA/MMT 0.5	6.28± 0.48	3.88±0.08	6.05±0.61
PLA/MMT 1	21.75 ± 2.14	4.50±0.14	10.05±0.90
PLA/MMT 2	16.70± 2.31	3.14±0.92	4.93±3.13
PLA/MMT 3	14.25 ± 3.20	2.74±0.16	2.85±0.49
PLA/gMA/MMT 1	78.45±30.34	5.84±0.06	11.95±0.74

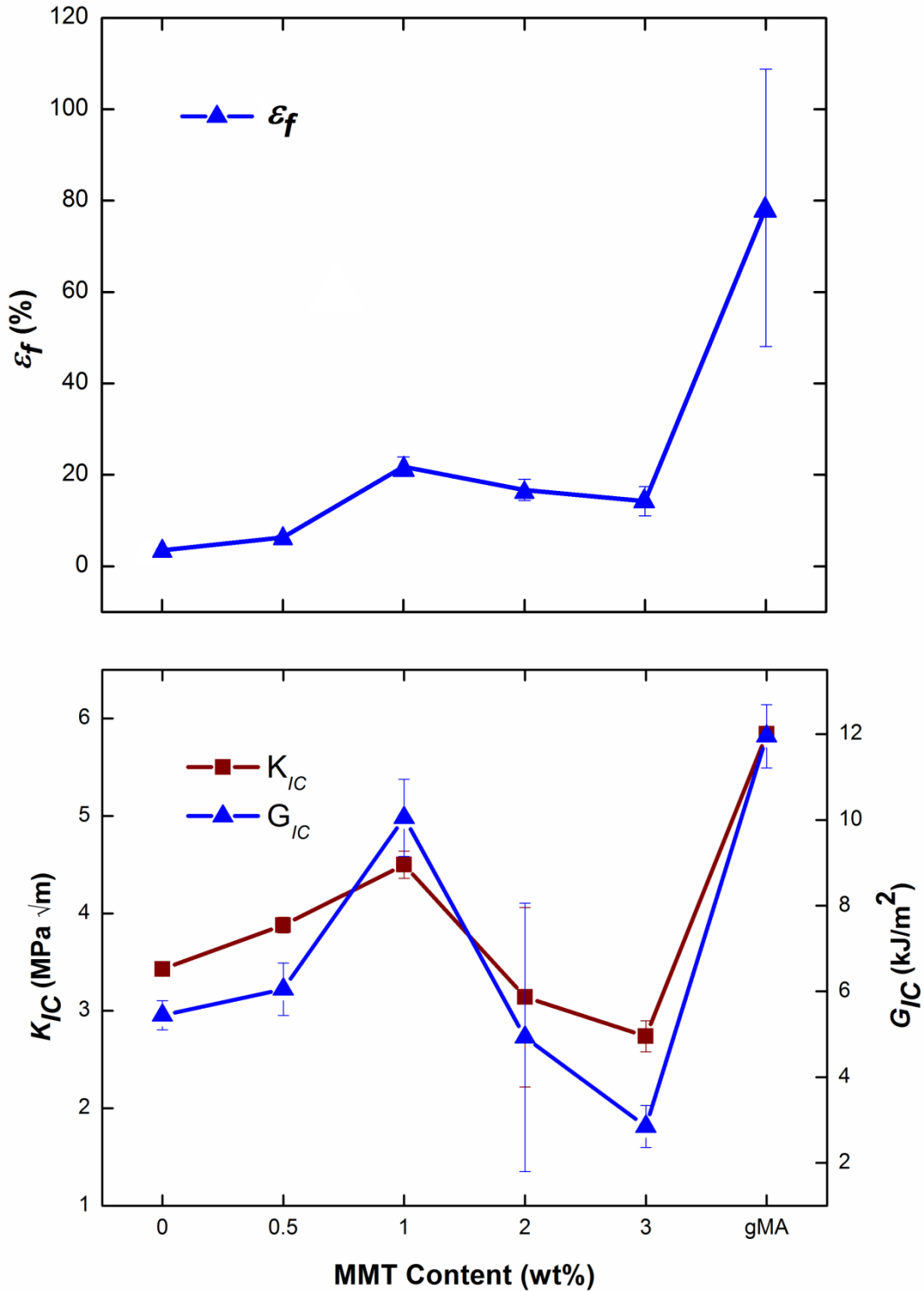


Figure 3.7 Effects of MMT content and MA compatibilization on the ductility (ϵ_f) and fracture toughness (K_{IC} and G_{IC}) of the specimens (note that gMA in the x-axes denotes PLA/gMA/MMT 1 specimen).

Moreover, morphology of the fracture surfaces of fracture toughness specimens were examined under SEM as given in Figure 3.8. It is seen that neat PLA has rather smooth fracture surface indicating its inherent brittleness. When MMT was incorporated Figure 3.8 indicates that fracture surface becomes rough with certain amount of plastic deformation lines, i.e. shear yielding, leading to increased fracture toughness values.

After MA compatibilization, it is seen in Figure 3.8 that fracture surface becomes very rough due to intensive level of plastic shear deformation decreasing the crack growth rate efficiently. Apart from “shearing” another important toughening mechanism would be “crack deflection” or “crack bowing” at the intercalated/exfoliated MMT layers distributed in the PLA matrix. Because, improved interfacial interaction via MA compatibilization would increase the efficiency of these toughening mechanisms.

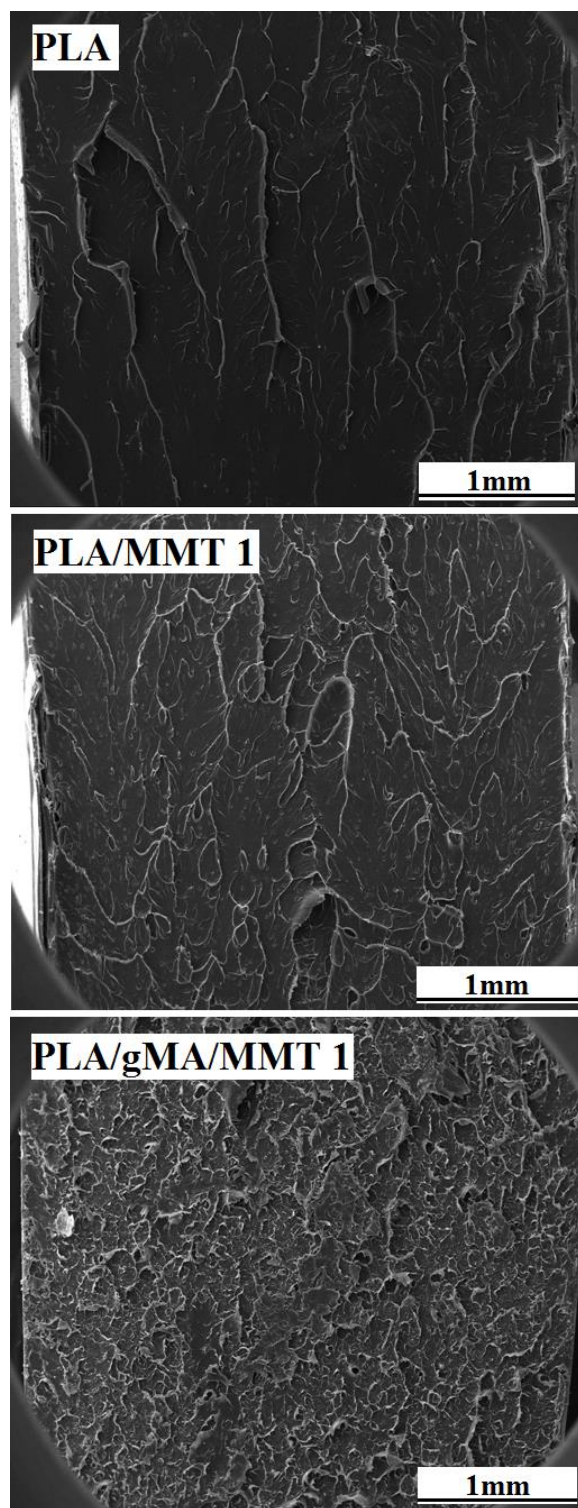


Figure 3.8 SEM fractographs showing fracture surface morphology of neat PLA and PLA/MMT nanocomposites.

3.1.5 Thermal Properties of the PLA/MMT Nanocomposites

Thermal properties of the nanocomposites were first evaluated by DSC analyses. Figure 3.9 shows first heating thermograms of the specimens after their injection molding operation, while Table 3.3 tabulates important transition temperatures: “glass transition, crystallization, melting” (T_g , T_c , T_m), “enthalpies of melting and crystallization” (ΔH_m and ΔH_c), and also “percent crystallinity” (X_C) of the specimens obtained using the following relation:

$$X_C = \frac{\Delta H_m - \Delta H_c}{w_{PLA} \Delta H_m^\circ} 100$$

In this relation, ΔH_m° represents melting enthalpy of 100% crystalline PLA determined as 93 J/g in the literature [72], while w_{PLA} represents weight fraction of the matrix PLA.

Table 3.3 indicates that incorporation of MMT with and without MA compatibilization have almost no effect on the glass transition and melting temperatures of the neat PLA. T_g of the neat matrix and its MMT nanocomposites appear at 63-65°C, while their T_m values are in the range 148-151°C.

The only difference observed was in the values of cold crystallization temperature; in which T_c of neat PLA (120 °C) could decrease as much as by 15°C with the incorporation of MMT. For instance, T_c of the nanocomposite specimen with 3 wt% MMT decreases to 105°C. This lower temperature start of cold crystallization with the presence of MMTs could be explained with their nucleation agent effect.

On the other hand, Table 3.3 also shows that the crystallinity amount of neat PLA was not affected by the presence of MMTs. Although, cold crystallization started at a lower temperature, the growth rate of the PLA spherulites could be hindered by the intercalated/exfoliated MMT layers preventing the required conformational mobility of the PLA chains to crystallize more.

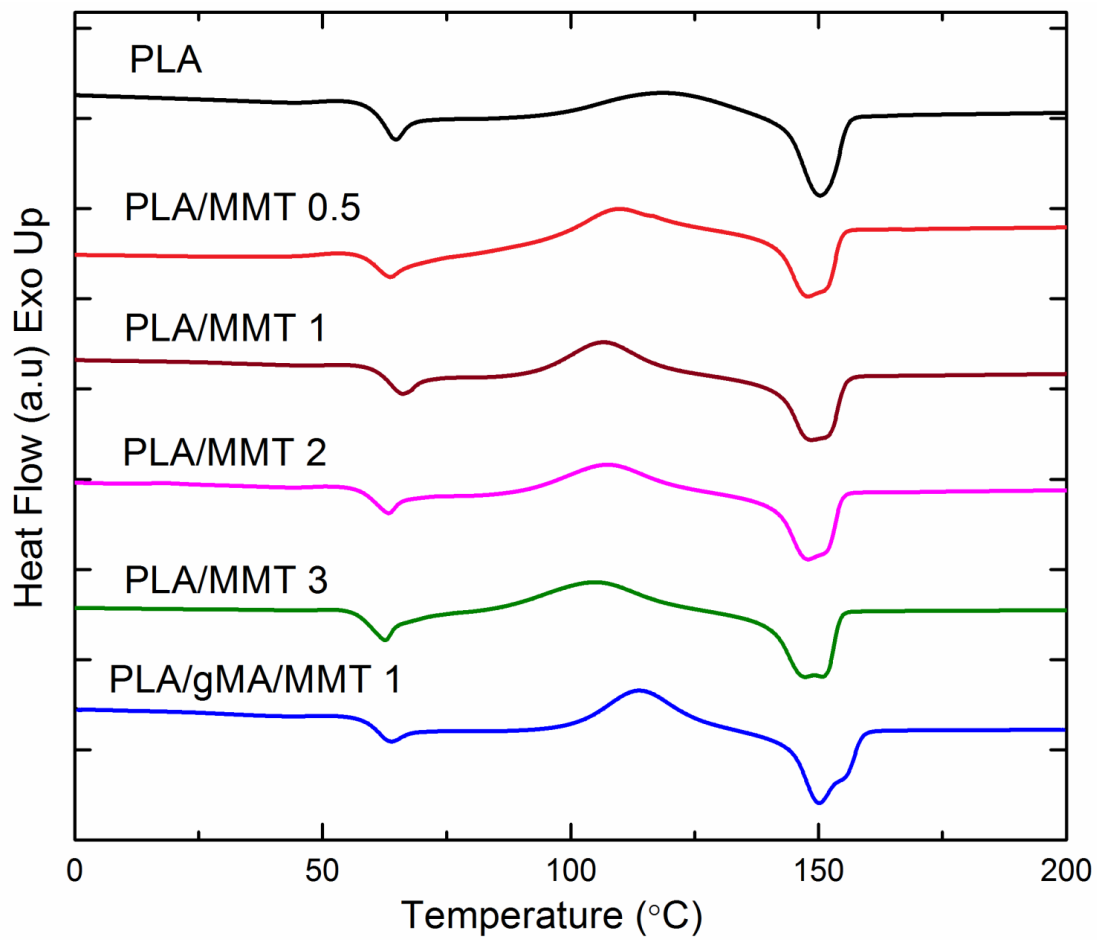


Figure 3.9 First heating DSC thermograms of the specimens.

Table 3.3 Transition Temperatures (T_g , T_c , T_m), Enthalpies (ΔH_m , ΔH_c) and Crystallinity Percent (X_C) of the Specimens During First Heating Profile

Specimens	T_g (°C)	T_c (°C)	T_m (°C)	ΔH_m (J/g)	ΔH_c (J/g)	X_C (%)
PLA	65	120	151	16.2	1.2	16.1
PLA/MMT 0.5	65	111	149	23.6	8.4	16.4
PLA/MMT 1	63	109	148	23.8	7.3	17.9
PLA/MMT 2	63	108	148	22.2	5.7	18.1
PLA/MMT 3	63	105	147	21.5	6.8	16.3
PLA/gMA/MMT 1	64	114	150	22.2	5.2	18.4

The second thermal analysis to investigate thermal degradation of the nanocomposites were thermogravimetric analysis (TGA) as given in Figure 3.10. Thermal degradation temperatures determined were tabulated in Table 3.4. In this table, $T_{5\%}$, $T_{10\%}$ and $T_{25\%}$ represent thermal degradation temperatures of the PLA and its MMT nanocomposites at 5, 10 and 25 wt% mass losses, while T_{max} represents the temperature at maximum mass loss. It was observed that use of MMT resulted in no significant improvements in the thermal degradation temperatures of the neat PLA; the increases were only a few degrees.

Table 3.4 Thermal Degradation Temperatures ($T_{5\%}$, $T_{10\%}$, $T_{25\%}$) of the Specimens at 5, 10 and 25 wt% Mass Losses and the Maximum Mass Loss Temperature (T_{max})

Specimens	$T_{5\%}$ (°C)	$T_{10\%}$ (°C)	$T_{25\%}$ (°C)	T_{max} (°C)
PLA	330	340	352	367
PLA/MMT 0.5	331	340	351	365
PLA/MMT 1	332	341	352	366
PLA/MMT 2	333	342	352	366
PLA/MMT 3	332	342	353	367
PLA/gMA/MMT 1	333	342	353	367

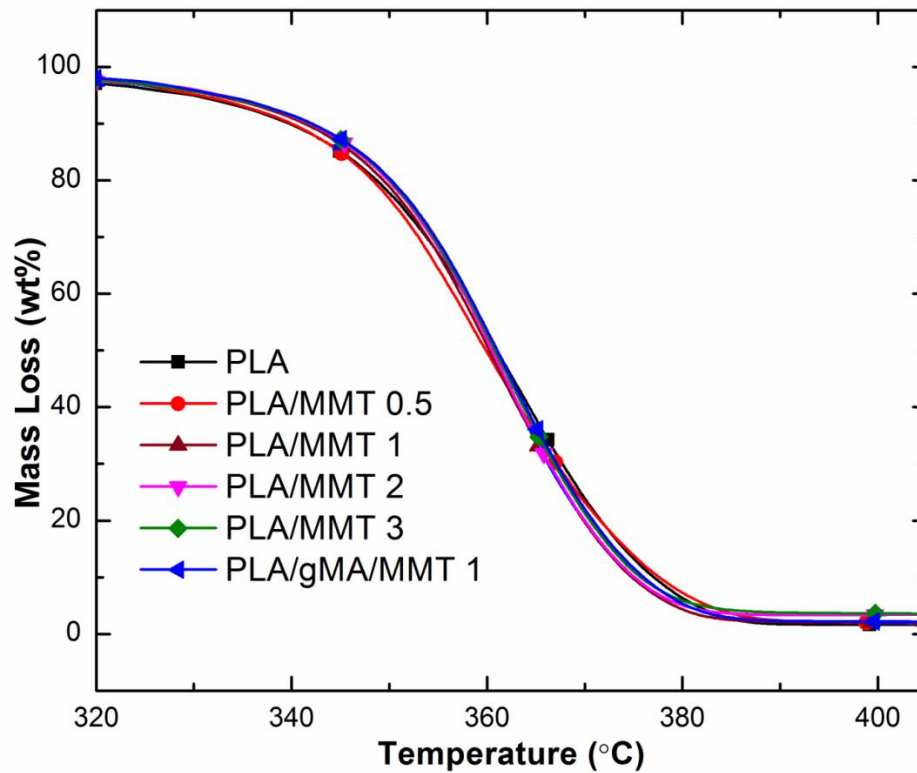


Figure 3.10 Thermogravimetric (TG) curves of the specimen.

3.2 Effects of Accelerated Weathering

Weathering performance of PLA and its 1 wt% MMT nanocomposite were determined by comparing the deteriorative effects of accelerated weathering on the color, molecular weight, chemical structure, mechanical properties and thermal behavior of the specimens. Influences on the MMT intercalation and PLA crystallization were also discussed in the following sections.

3.2.1 Effects on the MMT Intercalation

Mechanical and other properties of the polymer/MMT nanocomposites directly depend on the level of intercalation and/or exfoliation of the MMT layers via polymer chains. In this study, formation of PLA/MMT nanocomposite structure was investigated by XRD and TEM analysis.

Figure 3.11 shows that organically modified MMT used has an interlayer distance (d_{001}) of 1.8 nm which increases to 4.79 nm by the intercalation of macromolecular chains of PLA. TEM images in Figure 3.11 also reveal that MMT layers have both intercalated and exfoliated structure uniformly distributed in the matrix. Details of these analyses were discussed in the Section 3.1.1.

After weathering, due to the deteriorative actions of photodegradation and hydrolytic degradation on the PLA matrix, it can be expected that there would be certain level of collapse of intercalated and/or exfoliated MMT layers. On the other hand, Figure 3.11 reveals that even after accelerated weathering period of 200 h, no change was occurred in the 4.79 nm gallery distance of intercalated MMT layers. This can be interpreted that accelerated weathering parameters used in this study resulted in no change in the intercalated nanocomposite structure.

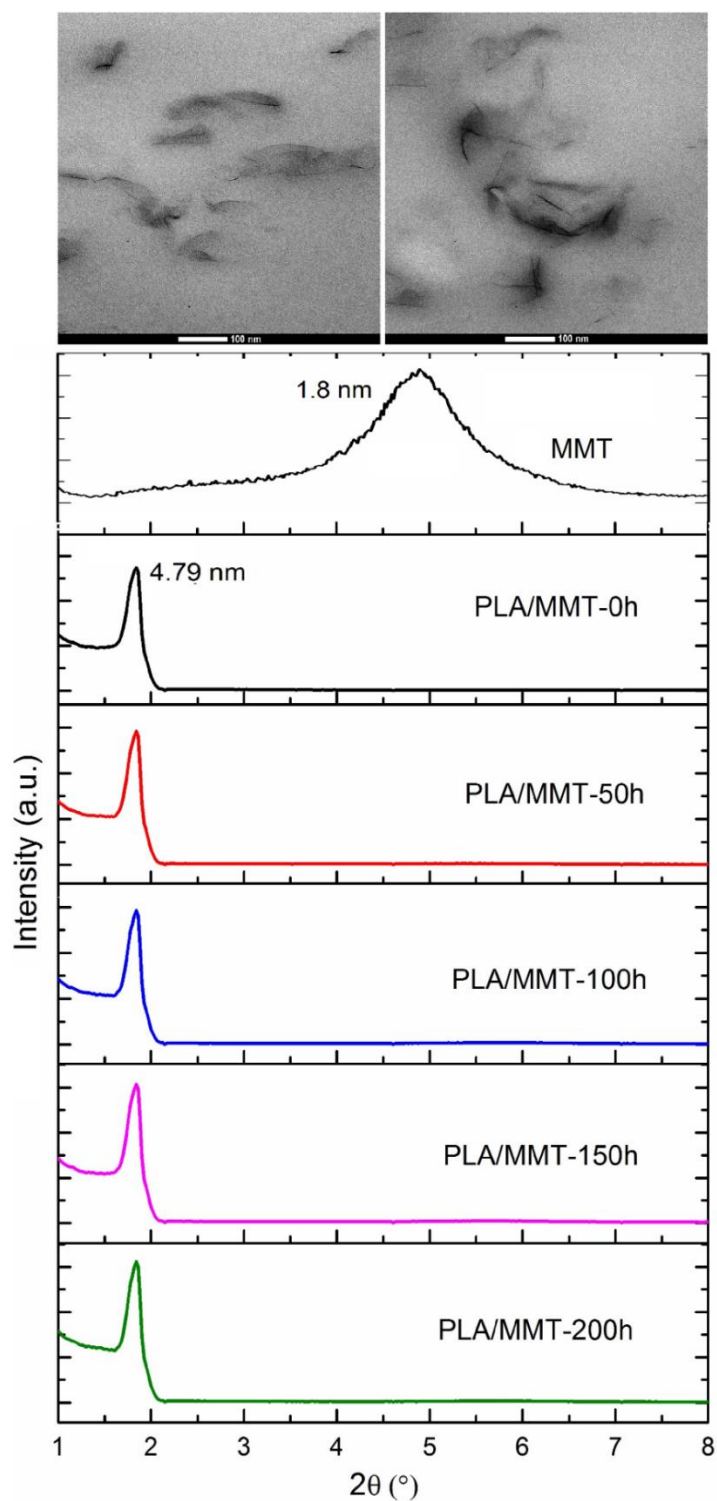


Figure 3.11 Effects of accelerated weathering periods on the XRD diffractograms showing intercalated nanocomposite structure, including TEM images of the intercalated and exfoliated MMT layers.

3.2.2 Effects on the PLA Crystallization

PLA is a partially crystalline biopolymer having a stable orthorhombic crystal structure named as α phase. It is known that (110)/(200) and (203) planes of α phase give XRD peaks at 2θ values of 16.3° and 18.7° , respectively [73-75].

However, PLA has very slow crystallization rate; thus, due to the very fast cooling rate during injection molding, macromolecular chains of PLA have no sufficient time to crystallize. Therefore, XRD curves of the unweathered specimens (i.e. PLA-0h and PLA/MMT-0h) on top of the Figure 3.12 have no sharp crystallization peaks, instead a very broad halo representing the mainly amorphous structure.

But, XRD diffractograms of the specimens after each accelerated weathering period in Figure 3.12 have very sharp peaks of α crystal phase at 2θ values of 16.3° and 18.7° . Because, both UV irradiation cycles taking place at 70°C and the shorter chains of PLA due to chain scission actions of degradation mechanisms provide sufficient energy and time required for the conformational mobility of PLA chains to crystallize.

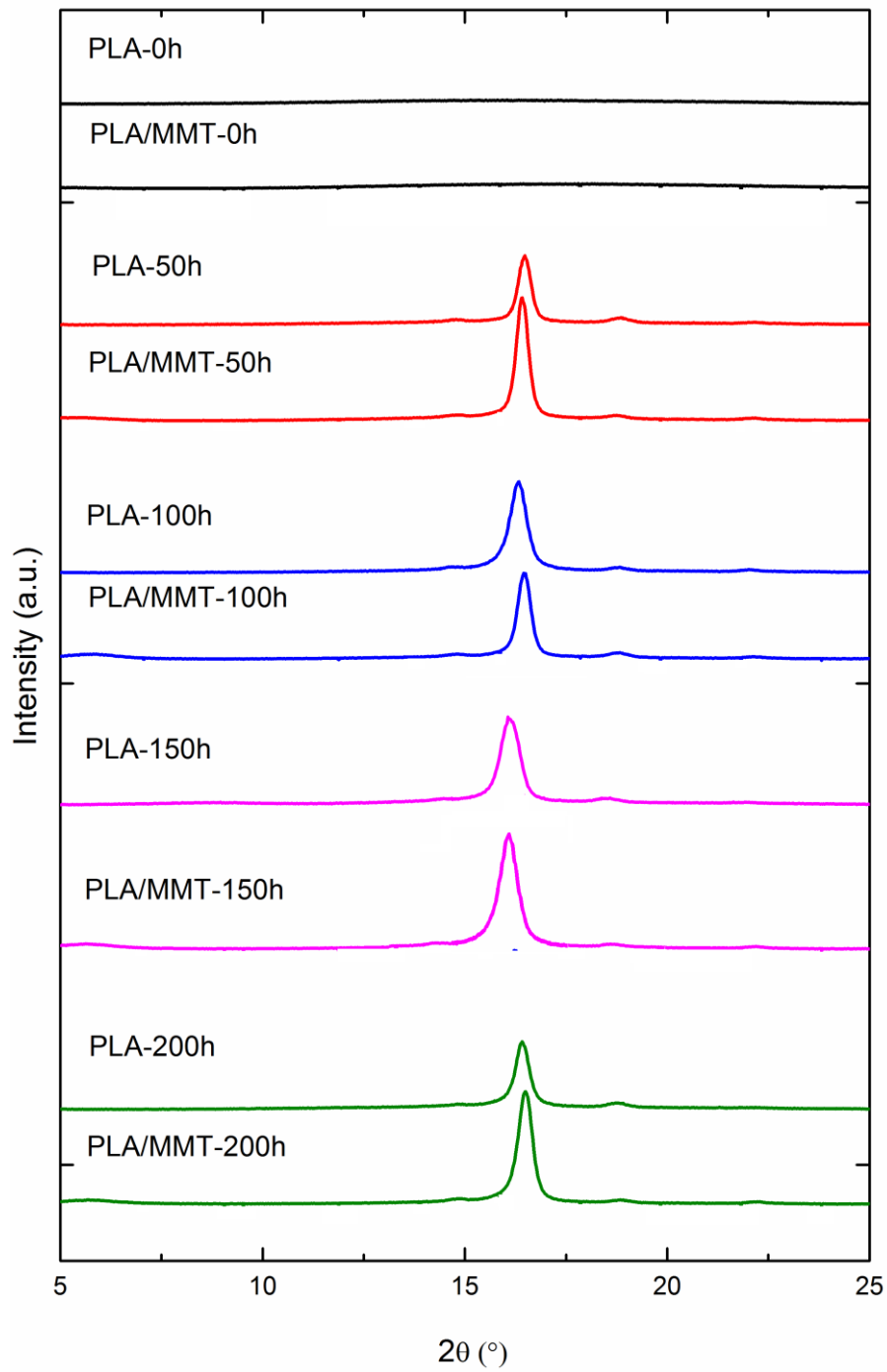


Figure 3.12 Effects of accelerated weathering periods on the XRD diffractograms of the specimens showing PLA crystallization.

3.2.3 Effects on the Color

In the outdoor applications, variation in the color of the polymeric components could be an important problem. Therefore, variation in the color of the specimens was first evaluated by comparing their photographic images after each accelerated weathering period.

It is seen in Figure 3.13 that neat PLA specimen appears colorless, i.e. very transparent due to the high degree of amorphous structure. Because, as discussed in the above section, very fast cooling rate of injection molding will not allow PLA chains to have conformational ability for crystallization. However, after 50 h accelerated weathering, neat PLA specimen became white due to the certain level of cold crystallization process occurred during weathering; and there was no significant change in its white color with further weathering periods of 100 h, 150 h and 200 h.

When 1 wt% MMT was added into PLA matrix, Figure 3.13 shows that nanocomposite specimen looks semitransparent with glossy yellowish color. After 50 h accelerated weathering, again due to the crystallization of PLA matrix, semitransparency was lost completely, and the specimen appears more yellowish. With further accelerated weathering periods, the variation in the color of PLA/MMT specimen was especially in the form of loss of glossy character.

In order to quantify variation in the color of the specimens, their color was also evaluated by comparing the CIELAB color space parameters L^* , a^* , b^* and the total color difference parameter ΔE^* . Table 3.5 tabulates these data of the specimens determined by diffused reflectance analysis (DRA) before and after each accelerated weathering period.

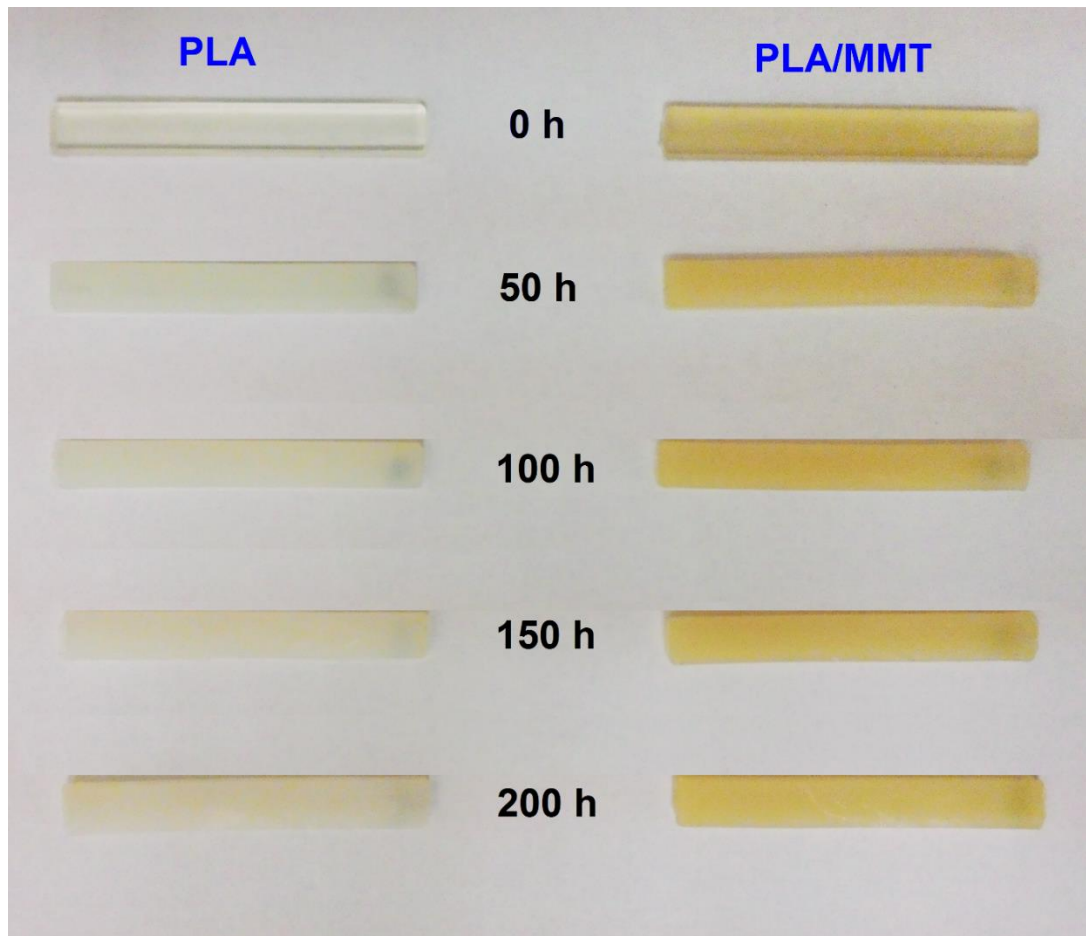


Figure 3.13 Effects of accelerated weathering periods on the photographic images of the specimens showing slight variation in the color.

Table 3.5 Effects of accelerated weathering periods on the CIELAB color space parameters (L^* , a^* , b^*) and color change difference (ΔE^*) values of the specimens

Specimens	L^*	a^*	b^*	ΔE^*
PLA-0h	16.71	-0.31	-0.64	
PLA/MMT-0h	23.49	-0.56	-1.53	
PLA-50h	22.49	-0.48	-3.26	6.34
PLA/MMT-50h	26.95	-0.75	-3.41	3.94
PLA-100h	23.22	-0.29	-3.05	6.94
PLA/MMT-100h	32.47	-0.74	-3.09	9.11
PLA-150h	22.41	-0.37	-3.71	6.47
PLA/MMT-150h	33.28	-0.60	-2.84	9.89
PLA-200h	22.38	-0.24	-3.93	6.55
PLA/MMT-200h	37.35	-0.61	-2.90	13.93

It is seen in Table 3.5 that the main variation for the neat PLA specimen takes place especially in the L^* color parameter related to “whiteness”, while for the PLA/MMT specimen variation takes place especially in the b^* color parameter related to “yellowness”. Table 3.5 also indicates that variation in these color parameters of L^* and b^* occur especially between the unweathered specimens and 50 h accelerated weathering specimens. Further accelerated weathering periods resulted in only very slight changes in these color parameters. That is, visual color variations observed in Figure 3.13 are in accordance with the quantitative color parameters tabulated in Table 3.5.

3.2.4 Effects on the Chemical Structure

The most significant variation in the chemical structure of the specimens during accelerated weathering via photodegradation and hydrolytic degradation mechanisms would be their random chain scission actions leading to decrease in the molecular weight of PLA matrix. Thus, the first analysis used was static light scattering (SLS) spectrometry to determine the level of chain scission in the PLA matrix after each accelerated weathering period.

SLS analysis revealed that weight average molecular weight (M_w) of the PLA matrix decreased from 3.7×10^5 g/mol to 2.7×10^5 after 50 h, then to 1.3×10^5 after 100 h, and to 1.0×10^5 after 150 h, and finally down to 0.8×10^5 after 200 h. As will be presented in the following sections, these successive reductions of M_w of PLA matrix with each accelerated weathering period led to consequent reductions in the mechanical properties of the specimens.

Secondly, in order to observe variation in the chemical structure of the specimens after weathering, IR analyses were performed. Figure 3.14 illustrates ATR-FTIR spectra of the neat PLA and its 1 wt% MMT nanocomposite before (0 h) and after each accelerated weathering periods (50 h, 100 h, 150 h, 200 h). The first spectrum in this figure reveals that PLA structure can be identified basically by five characteristic IR bands: C-C stretching peak at 867 cm^{-1} , C-O stretching peaks at 1079, 1126, 1181 and 1264 cm^{-1} , C-H deformation peaks at 1377 and 1452 cm^{-1} , C=O ester carbonyl groups at 1748 cm^{-1} , and C-H stretching peaks at 2853 and 2924 cm^{-1} . These band assignments are all in accordance with the IR bands discussed in the literature [15, 39].

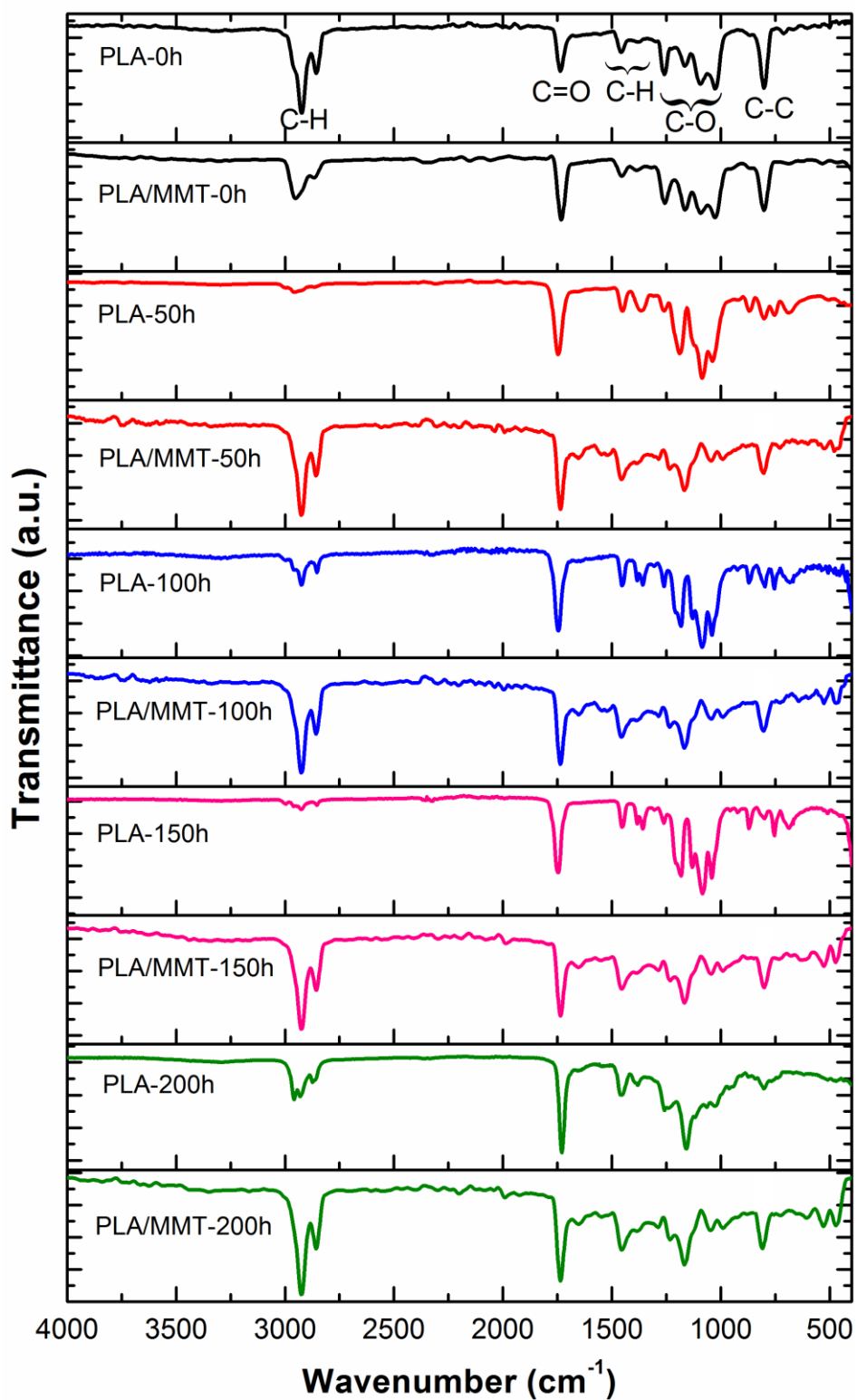


Figure 3.14 Effects of accelerated weathering periods on the ATR-FTIR spectra of the specimens showing variation in the chemical structure.

As stated in the introduction part, UV irradiation deteriorates the structure of PLA via photodegradation mechanisms of “Norrish II type photocleavage”, “photolysis” and “photooxidation” [12, 15, 39, 40, 55-57].

Photolysis leads to chain scission especially in the C-O bonds of the PLA ester backbone structure by absorption of a photon. After weathering, it is discussed that IR bands of C-O stretching peaks either decrease or shift to lower wavenumbers. Figure 3.14 shows that intensity of these bands not only decrease but also shift to lower wavenumbers especially after 200 h of weathering. These shifts of the C-O peaks for the neat PLA specimen are from 1079 to 1027 cm^{-1} , from 1126 to 1064 cm^{-1} , from 1181 to 1160 cm^{-1} , and from 1264 to 1239 cm^{-1} ; while for the PLA/MMT specimen from 1025 to 990 cm^{-1} , from 1088 to 1046 cm^{-1} , from 1166 to 1164 cm^{-1} , and from 1257 to 1231 cm^{-1} .

Norrish II type photocleavage takes place at the ester group and ethylidene group next to the ester oxygen in the PLA structure leading to chain cleavage and the formation of C=C double bonds and carboxylic acid -OH stretching [40, 57]. Photooxidation of PLA results in formation of hydroperoxide derivative and its subsequent degradation into carboxylic acid and diketone end groups [40, 57]. Therefore after weathering, it is discussed that intensity of the IR band of C=O bond either increase or shift to lower wavenumbers. Figure 3.14 indicates that for both PLA and PLA/MMT specimens especially after 200 h of accelerated weathering, there is substantial increase in the intensity of the C=O bond, and also shifting from 1748 cm^{-1} to 1729 cm^{-1} for neat PLA, and from 1741 cm^{-1} to 1735 cm^{-1} for PLA/MMT specimen.

Bocchini et al. [12, 56] also proposed that a series of radical photooxidation reactions of PLA could lead to formation of anhydride groups appearing as an IR band at 1845 cm^{-1} . In this study, this band was only observed as extremely tiny broad forms, but not as clear peaks.

Besides UV radiation at 70°C, another important step during accelerated weathering tests was the humidity (condensation) steps at 50°C. Apart from swelling and plasticization, the main degradation mechanism of humidity is defined as “hydrolysis”. It is known that hydrolysis also contributes to main chain scission especially in the C-O bonds of the ester structure of PLA [41, 42]. It was also indicated that, just like photo-oxidation, hydrolysis might also lead to formation of carboxylic acid and ketone end groups. Therefore, variations in the IR spectra of the specimens due to hydrolysis would be very similar to the variations discussed before.

3.2.5 Effects on the Fracture Surface Morphology

Effects of each accelerated weathering period on the variation of the fracture surface morphology of neat PLA and PLA/MMT specimens were examined by comparing the SEM images of the fracture surface of their fracture toughness test specimens. Figure 3.15 shows that due to severe chemical degradation in the structure of neat PLA specimen, extensive number of voids, cracks and cleavages can be observed on the fracture surface. Therefore, its rather smooth fracture surface before weathering becomes extremely rough after each accelerated weathering period.

On the other hand, it is seen in Figure 3.15 that the number of voids and cracks were not extensive on the fracture surface of PLA/MMT specimen. Therefore, as will be discussed in the next section, compared to mechanical properties of neat PLA, use of PLA/MMT nanocomposite was much more beneficial both before weathering and after 200 h accelerated weathering.

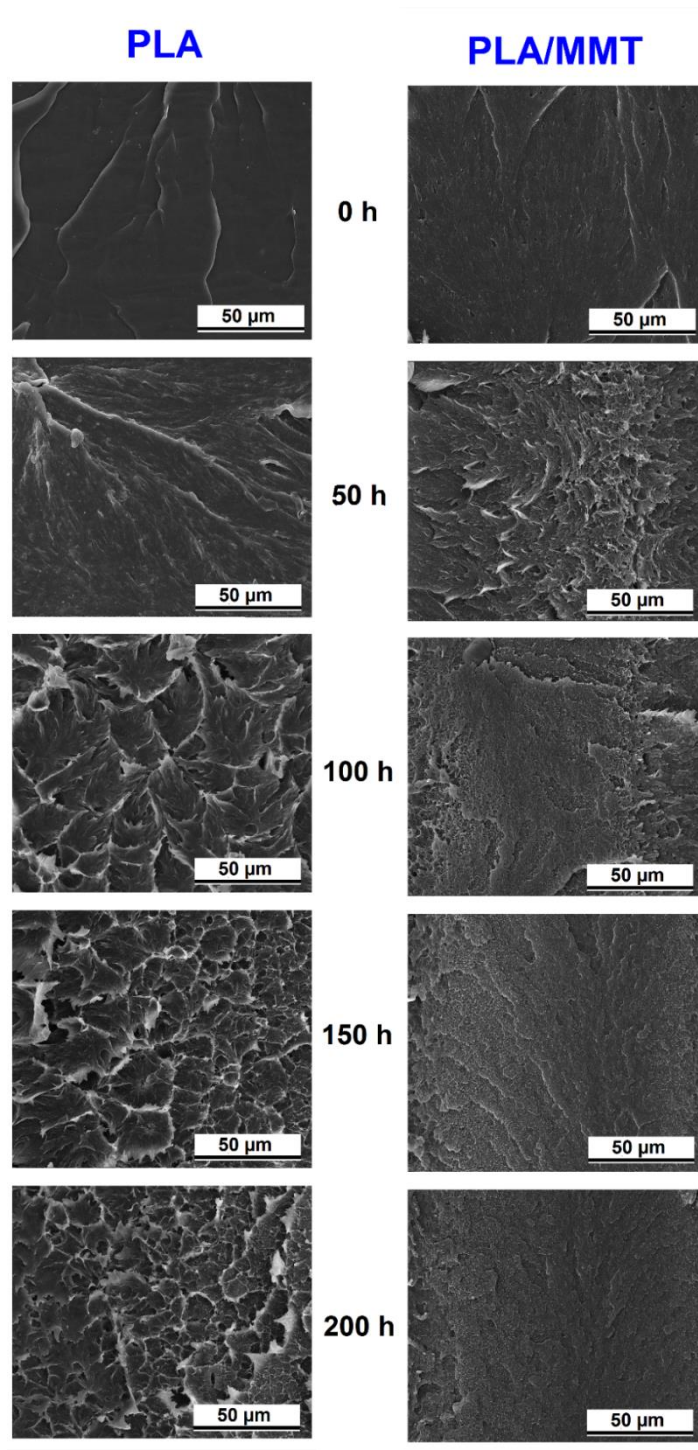


Figure 3.15 Effects of accelerated weathering periods on the SEM images of the specimens showing variation in the fracture surface morphology.

3.2.6 Effects on the Mechanical Properties

Effects of accelerated weathering on the variation in modulus and strength of PLA and PLA/MMT nanocomposite specimens were determined first by three point bending tests and then also by tension tests. Figure 3.16 and 3.17 illustrate variations in “flexural stress-strain” and “tensile stress-strain” curves at each accelerated weathering period; while Table 3.6 tabulates values of “Flexural and Tensile Modulus (E_{Flex} and E)” and “Flexural and Tensile Strength (σ_{Flex} and σ_{TS})” determined from these curves. Moreover, influences of accelerated weathering periods on the modulus and strength values of the specimens are also evaluated in Figure 3.18.

Table 3.6 Effects of accelerated weathering periods on the flexural modulus (E_{Flex}), tensile modulus (E), flexural strength (σ_{Flex}) and tensile strength (σ_{TS}) of the specimens

Specimens	E_{Flex} (GPa)	E (GPa)	σ_{Flex} (MPa)	σ_{TS} (MPa)
PLA-0h	3.60±0.07	2.85±0.08	97.9±1.3	58.6±1.4
PLA/MMT-0h	4.18±0.10	3.17±0.08	104.2±1.3	61.0±0.6
PLA-50h	4.58±0.09	2.89±0.16	93.0±1.9	51.6±1.1
PLA/MMT-50h	5.03±0.06	3.19±0.22	127.6±2.3	62.65±1.3
PLA-100h	4.51±0.01	2.86±0.18	82.8±0.2	39.1±0.6
PLA/MMT-100h	4.93±0.09	2.98±0.10	115.7±2.3	55.75±3.5
PLA-150h	4.21±0.04	2.73±0.09	57.7±2.7	29.5±1.2
PLA/MMT-150h	4.90±0.30	2.77±0.17	105.8±4.1	43.86±2.7
PLA-200h	4.12±0.13	2.43±0.13	52.3±0.6	22.8±1.5
PLA/MMT-200h	4.85±0.10	2.69±0.10	98.4±7.9	32.01±1.1

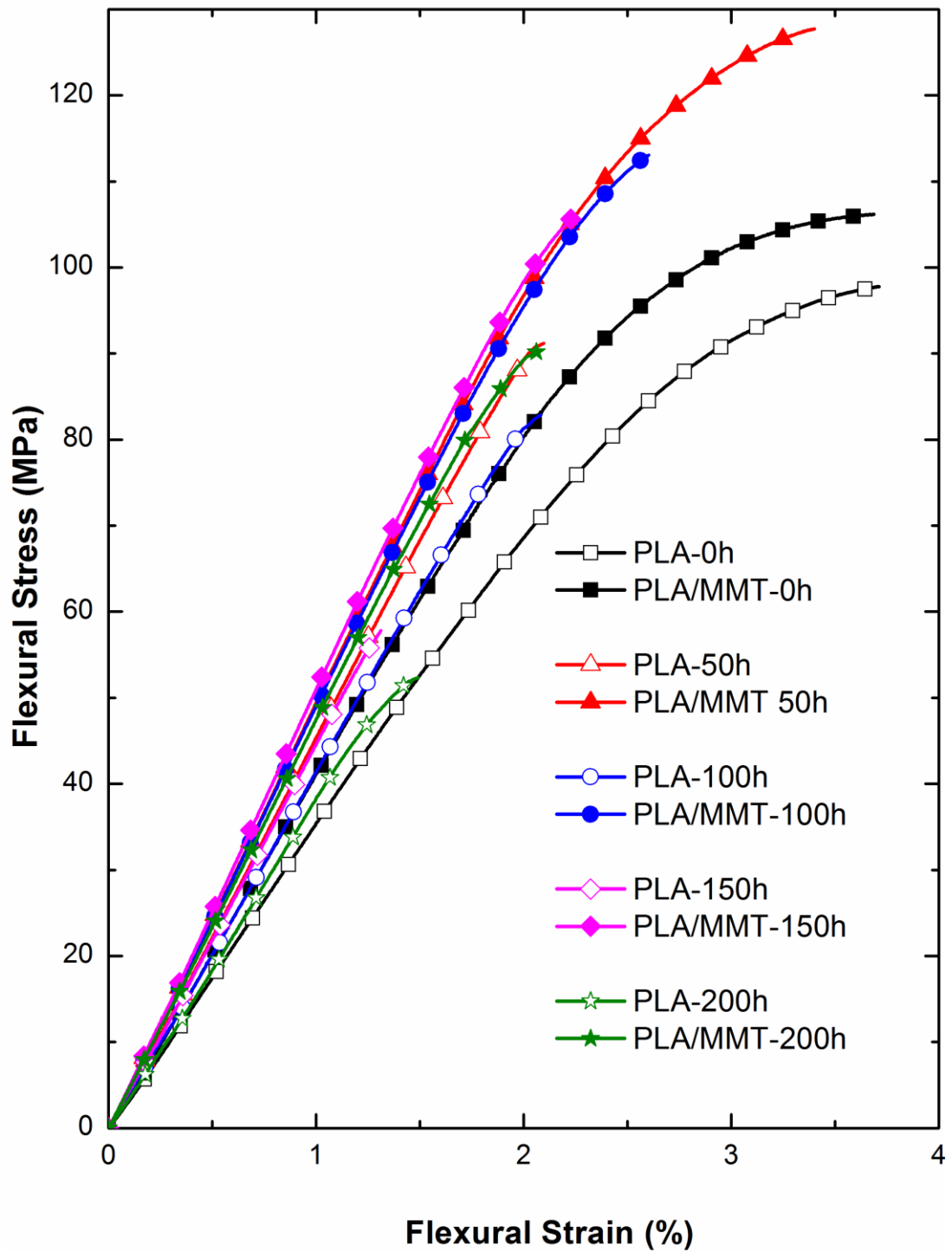


Figure 3.16 Effects of accelerated weathering periods on the flexural stress-strain curves of the specimens.

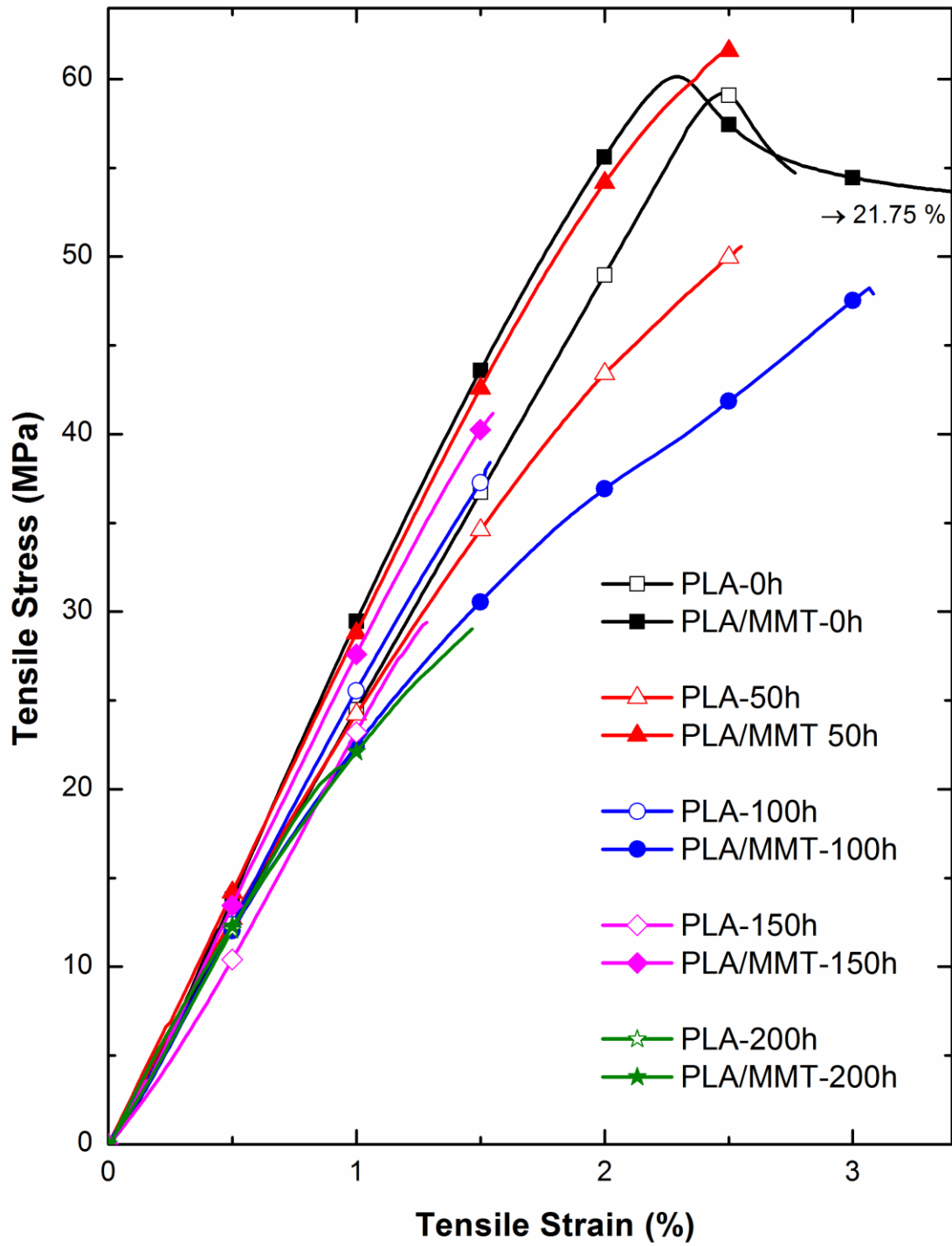


Figure 3.17 Effects of accelerated weathering periods on the tensile stress-strain curves of the specimens.

It is seen in Table 3.6 and Figure 3.18 that both elastic modulus values (especially E_{Flex}) of neat PLA and its 1 wt% MMT nanocomposite increase after 50 h of accelerated weathering. For example, the increase in E_{Flex} values for neat PLA is 27%, while it is 20% for the PLA/MMT nanocomposite. As discussed before, these increases were due to the increased crystallinity of the PLA matrix. Because, unweathered injection molded PLA structure is mainly amorphous. During weathering, UV irradiation cycles at 70°C resulted in cold crystallization of PLA chains.

On the other hand, during accelerated weathering beyond 50 h, chemical degradation due to photolysis, photooxidation and hydrolysis was more dominant than the stiffening action of the crystallinity. Therefore, after 50 h both elastic modulus values (E_{Flex} and E) started to decrease gradually. For instance, after 200 h, compared to the tensile modulus values of the unweathered specimens, the decreases in E values were 6% for PLA, and 15% for PLA/MMT specimens. However, E_{Flex} values after 200 h were still slightly over the E_{Flex} values of the unweathered PLA and PLA/MMT specimens.

A similar variation trend was observed for both strength values (especially σ_{Flex}) of the PLA/MMT nanocomposite specimen. Table 3.6 and Figure 3.18 show that after 50 h accelerated weathering compared to the unweathered one, tensile strength (σ_{TS}) of the nanocomposite was slightly over, while its flexural strength (σ_{Flex}) increased as 23%. These increases were not just benefits of higher crystallinity, but also due to the additional composite strengthening mechanisms. That is, “decrease of mobility” of PLA chains and “load transfer” from the PLA matrix to intercalated/exfoliated MMT layers. However, beyond accelerated weathering of 50 h, decrease of M_w of the PLA matrix was dominant leading to gradual decrease in the strength values at each period successively. At the end of 200 h weathering, compared to unweathered PLA/MMT nanocomposite, the decrease in σ_{TS} was 51%, while in σ_{Flex} only 6%.

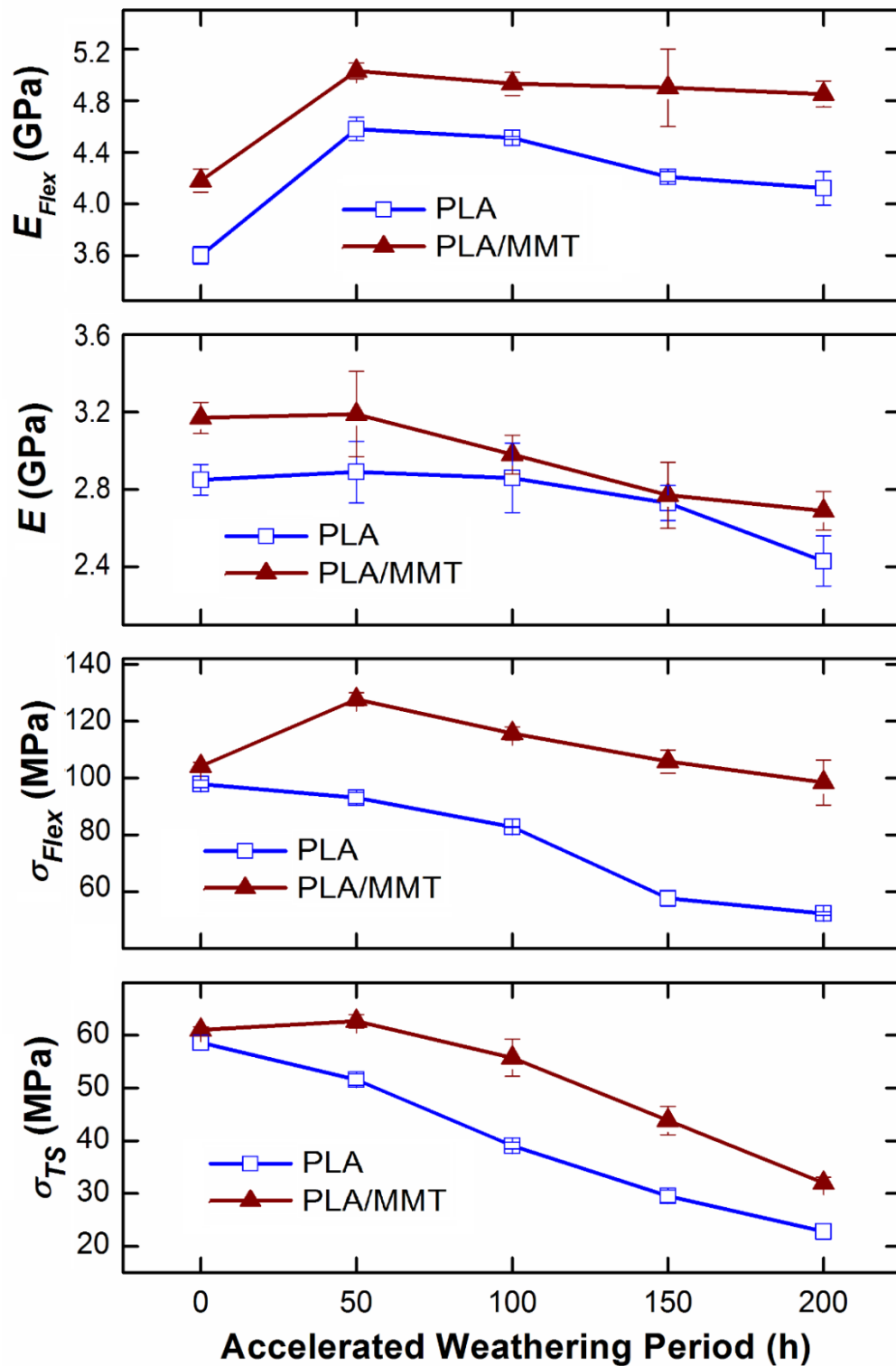


Figure 3.18 Effects of accelerated weathering periods on the flexural and tensile modulus, and flexural and tensile strength of the specimens.

However, as shown in Table 3.6 and Figure 3.18, increase in the crystallinity of PLA was not sufficient to keep the strength (both σ_{Flex} and σ_{TS}) values of the unweathered neat PLA specimen. Severe actions of chain scission resulted in the gradual decreases of strength values after each accelerated weathering period successively. At the end of 200 h total accelerated weathering, σ_{Flex} of neat PLA decreased 47%, while this decrease in σ_{TS} was 61%.

Variation in ductility of PLA and PLA/MMT nanocomposite specimens at each weathering period were evaluated by comparing their “%final strain at break” (ϵ_f) values. These data were determined from their tensile stress-strain curves given in Figure 3.17; then the values are tabulated in Table 3.7 and compared at each weathering period in Figure 3.19. It is clearly seen that ϵ_f values of each specimen drastically drop at 50 h, and then continue to decrease successively with increasing accelerated weathering period. After 200 h of total weathering, drops in ϵ_f were 69% for PLA and 94% for PLA/MMT, respectively. Decreases in the ductility of the specimens, that is decreases in the ability of the specimens to have permanent plastic deformation up to fracture, are again due to the deteriorated molecular weight of the PLA matrix.

Variation in the toughness of neat PLA and its 1 wt% MMT nanocomposite specimens at each weathering period were investigated by comparing their fracture toughness values in terms of “Critical Stress Intensity Factor (K_{IC})” and “Critical Strain Energy Release Rate (G_{IC})” (Table 3.7 and Figure 3.19). It is known that K_{IC} and G_{IC} values are important in terms of the ability of the materials to hinder initiation and propagation of cracks leading to fracture.

Table 3.7 Effects of accelerated weathering periods on the tensile strain at break (ϵ_f) and fracture toughness (K_{IC} and G_{IC}) of the specimens

Specimens	ϵ_f (%)	K_{IC} (MPa \sqrt{m})	G_{IC} (kJ/m ²)
PLA-0h	3.48±0.25	3.43±0.04	5.44±0.34
PLA/MMT-0h	21.75 ± 2.14	4.50±0.14	10.05±0.90
PLA-50h	2.39±0.19	3.50±0.04	5.94±0.16
PLA/MMT-50h	3.37±0.18	5.15±0.14	10.67±0.23
PLA-100h	1.51±0.15	3.37±0.01	4.93±0.64
PLA/MMT-100h	3.09±0.05	4.09±0.09	8.16±0.69
PLA-150h	1.18±0.10	3.03±0.06	4.24±0.72
PLA/MMT-150h	1.90±0.24	3.94±0.21	7.77±0.20
PLA-200h	1.08±0.09	2.68±0.05	3.45±0.54
PLA/MMT-200h	1.90±0.18	3.55±0.01	5.78±0.09

Table 3.7 and Figure 3.19 indicate that, except very slight increases in the K_{IC} and G_{IC} values of PLA and PLA/MMT specimens after 50 h accelerated weathering (due to the higher crystallinity), their fracture toughness values all decreased successively with increasing weathering period. At the end of the 200 h total accelerated weathering, decreases in the K_{IC} and G_{IC} values of neat PLA were 22% and 37%, respectively; while for the PLA/MMT nanocomposite these decreases were 27% and 50%, respectively. The possible reason for the higher level of decrease in the nanocomposite specimen would be the chemical degradation occurring not only in the PLA matrix

material, but also in the interfacial interactions between the matrix and intercalated/exfoliated MMT layers, which prevented certain composite toughening mechanisms, such as “crack deflection”.

Lastly, in order to reveal benefits of using PLA/MMT nanocomposite rather than neat PLA, all the mechanical properties of these two specimens before weathering (0 h) and after total 200 h of accelerated weathering period are tabulated in Table 3.8. Note that benefits of using PLA/MMT-0h and PLA/MMT-200h nanocomposite specimens compared to PLA-0h and PLA-200h specimens are tabulated in terms of “% benefit at 50 h” and “% benefit at 200 h”, respectively.

According to the data given in Table 3.8 it can be deduced that in terms of mechanical properties, rather than neat PLA use of PLA with only 1 wt% MMT is extremely beneficial not only under normal conditions, but also under severe atmospheric weathering conditions, i.e. not only for “indoor applications” but also for “outdoor applications”.

For example, flexural modulus and strength (E_{Flex} and σ_{Flex}) were 16% and 6% beneficial before weathering, but after weathering these benefits were 18% and 88%, respectively. $\% \varepsilon_f$ ductility before weathering was more than 5 times beneficial, after weathering 76% beneficial. Benefits in G_{IC} fracture toughness before and after weathering were 85% and 68%, respectively.

Benefits of nanocomposite use were not only due to the very effective nanoscale reinforcing actions of intercalated/exfoliated MMT layers, but also due to their effective barrier actions decreasing the detrimental effects of photodegradation and hydrolytic degradation.

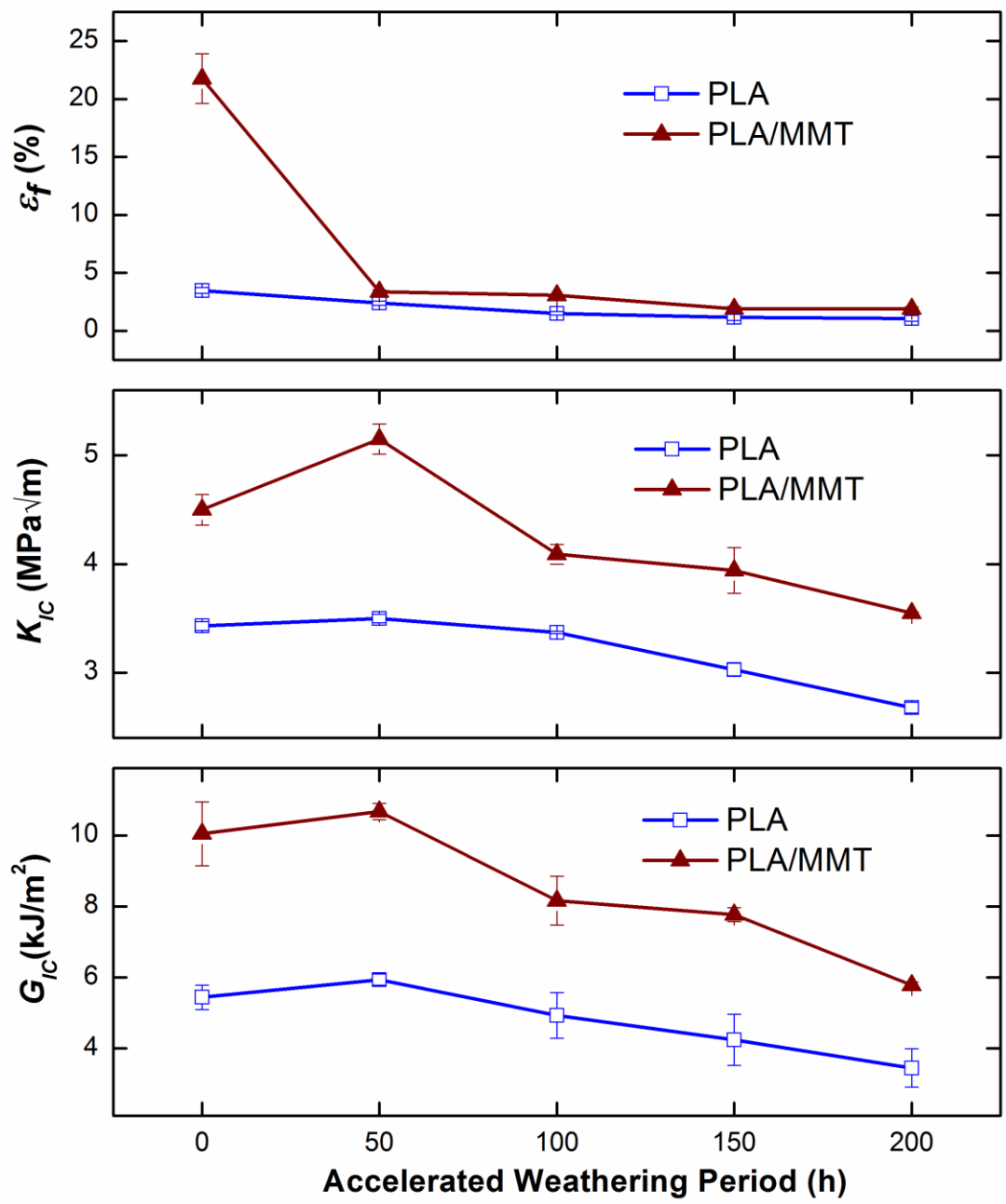


Figure 3.19 Effects of accelerated weathering periods on the ductility and fracture toughness of the specimens.

Table 3.8 Comparison of the mechanical properties of neat PLA and PLA/MMT nanocomposite specimens before (0 h) and after (200 h) accelerated weathering, including the “% benefit” (percent increase in the values) of the nanocomposite specimen at 0 h and 200 h.

Mechanical Properties	PLA at 0h	PLA/MMT at 0h	Benefits at 0h	PLA at 200h	PLA/MMT at 200h	Benefits at 200h
Tensile Modulus E (GPa)	2.85	3.17	11%	2.43	2.69	11%
Flexural Modulus E_{Flex} (GPa)	3.60	4.18	16%	4.12	4.85	18%
Tensile Strength σ_{TS} (MPa)	58.6	61.0	4%	22.80	32.01	40%
Flexural Strength σ_{Flex} (MPa)	97.9	104.2	6%	52.30	98.40	88%
Tensile Strain at Break ε_f (%)	3.48	21.75	525%	1.08	1.9	76%
Fracture Toughness K_{IC} (MPa \sqrt{m})	3.43	4.50	31%	2.68	3.55	33%
Fracture Toughness G_{IC} (kJ/m ²)	5.44	10.05	85%	3.45	5.78	68%

3.2.7 Effects on the Thermal Behavior

First of all variation in the thermal behavior of neat PLA and PLA/MMT nanocomposite specimens at each accelerated weathering period were investigated by DSC analyses. DSC thermograms obtained during first heating profile are given in Figure 3.20, while “glass transition, crystallization, melting” (T_g , T_c , T_m) temperatures; “enthalpies of melting and crystallization” (ΔH_m and ΔH_c), and also “percent crystallinity” (X_C) of the specimens are tabulated in Table 3.9. X_C is determined using ΔH_m , ΔH_c and ΔH_m° which is the melting enthalpy of 100% crystalline PLA determined as 93 J/g in the literature [72].

It is seen in Figure 3.20 and Table 3.9 that there were no significant variation in the glass transition and melting temperatures of the PLA matrix at each weathering period. The only fundamental variation in the first heating DSC thermograms appeared as the loss of exothermic cold crystallization (ΔH_c) peaks. Since cooling rate of injection molding is very fast, crystallinity amount (X_C) for the unweathered neat PLA was 16%, similarly for the PLA/MMT matrix it was 18%. However, during accelerated weathering, UV irradiation cycles at 70°C lead to more energy and time for the conformational mobility of PLA chains to crystallize even more. Thus, Table 3.9 shows that X_C of each specimen during weathering periods increased to around 30%, i.e. they are almost doubled.

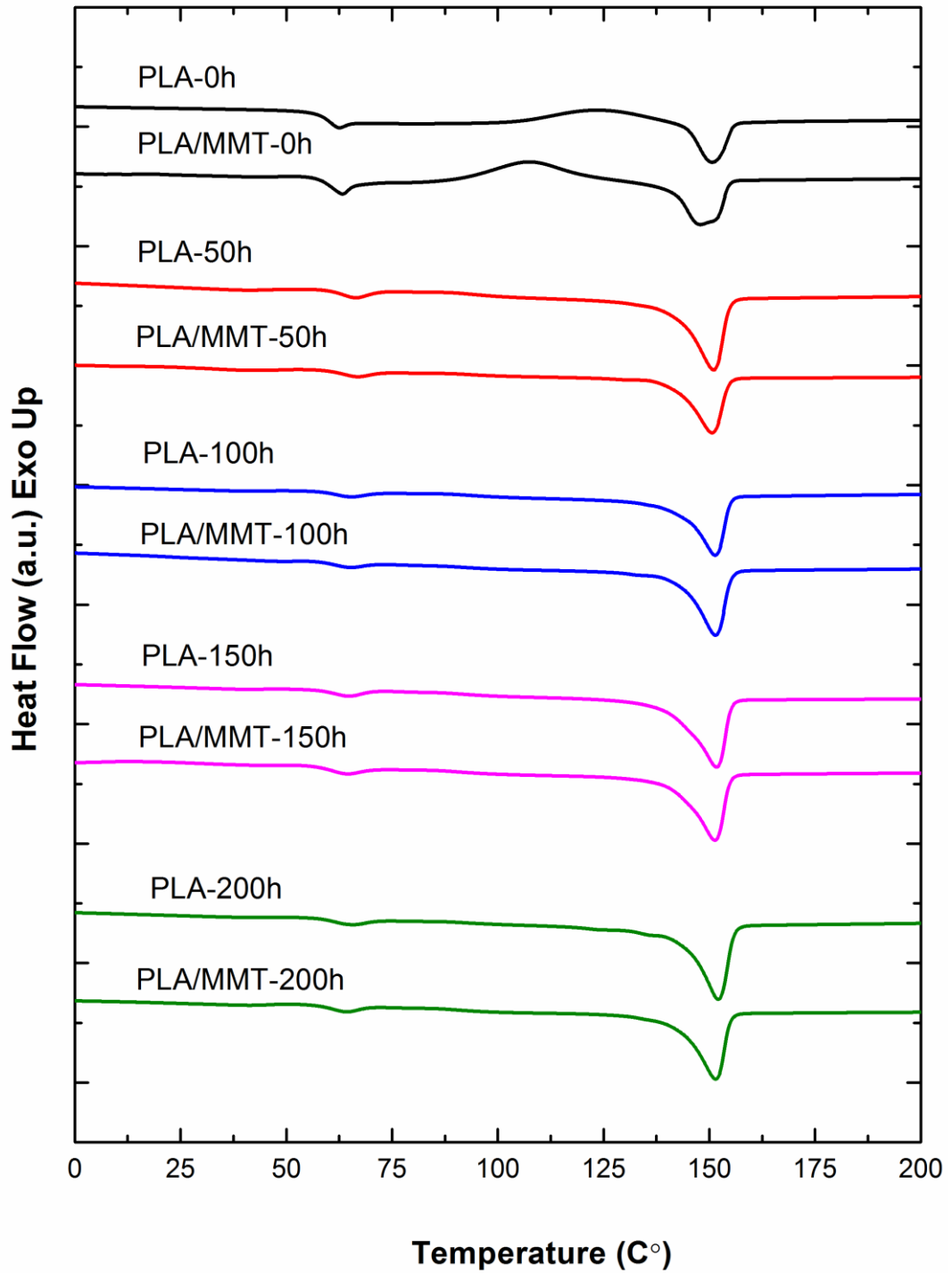


Figure 3.20 Effects of accelerated weathering periods on the first heating DSC thermograms of the specimens.

Table 3.9 Effects of accelerated weathering periods on the transition temperatures (T_g , T_c , T_m), enthalpies (ΔH_m , ΔH_c) and crystallinity percent (X_C) of the specimens

Specimens	T_g (°C)	T_c (°C)	T_m (°C)	ΔH_m (J/g)	ΔH_c (J/g)	X_C (%)
PLA-0h	65	120	151	16.2	1.2	16.1
PLA/MMT-0h	63	109	148	23.8	7.3	17.9
PLA-50h	66	-	151	30.5	-	32.8
PLA/MMT-50h	67	-	150	26.1	-	28.3
PLA-100h	65	-	151	28.5	-	30.6
PLA/MMT-100h	65	-	152	25.1	-	27.3
PLA-150h	65	-	151	28.2	-	30.3
PLA/MMT-150h	64	-	151	27.2	-	29.5
PLA-200h	65	-	152	27.9	-	30.0
PLA/MMT-200h	64	-	152	28.1	-	30.5

Of course the increase in the matrix crystallinity of the specimens would be not only due to the UV irradiation at 70°C, but also due to the severe chain scission actions of photodegradation and hydrolytic degradation leading to decreased M_w of the matrix. Therefore, since shorter PLA chains would be more mobile, then the conformational requirement for the ordered crystalline structure would be easier.

As the second thermal analysis, in order to determine variation in the thermal degradation temperatures of neat PLA and PLA/MMT nanocomposite specimens at each accelerated weathering period, TGA was conducted. Thermogravimetric curves and thermal degradation temperatures determined from these curves for each specimen are given in Figure 3.21 and Table 3.10, respectively. In this table, $T_{5\%}$, $T_{10\%}$ and $T_{25\%}$ denote thermal degradation temperatures of the specimens at 5, 10 and 25 wt% mass losses, while T_{max} denotes the temperature at maximum mass loss.

Figure 3.21 and Table 3.10 indicate that there was no significant variation in the thermal degradation behavior of each specimen during each accelerated weathering period, basically due to the higher crystallinity of the PLA matrix as discussed before. There were only slight decreases (2-4°C) in the onset temperatures of thermal degradation, i.e. in the values of $T_{5\%}$ and $T_{10\%}$ for the neat PLA specimen, but not for the PLA/MMT nanocomposite specimen.

Table 3.10 Effects of accelerated weathering periods on the thermal degradation temperatures ($T_{5\%}$, $T_{10\%}$, $T_{25\%}$) of the specimens at 5, 10 and 25 wt% mass losses and the maximum mass loss temperature (T_{max})

Specimens	$T_{5\%}$ (°C)	$T_{10\%}$ (°C)	$T_{25\%}$ (°C)	T_{max} (°C)
PLA-0h	330	340	352	367
PLA/MMT-0h	332	341	352	366
PLA-50h	321	333	347	365
PLA/MMT-50h	330	340	352	361
PLA-100h	327	339	352	367
PLA/MMT-100h	330	340	352	361
PLA-150h	326	339	352	367
PLA/MMT-150h	326	337	350	360
PLA-200h	326	338	352	367
PLA/MMT-200h	330	340	352	360

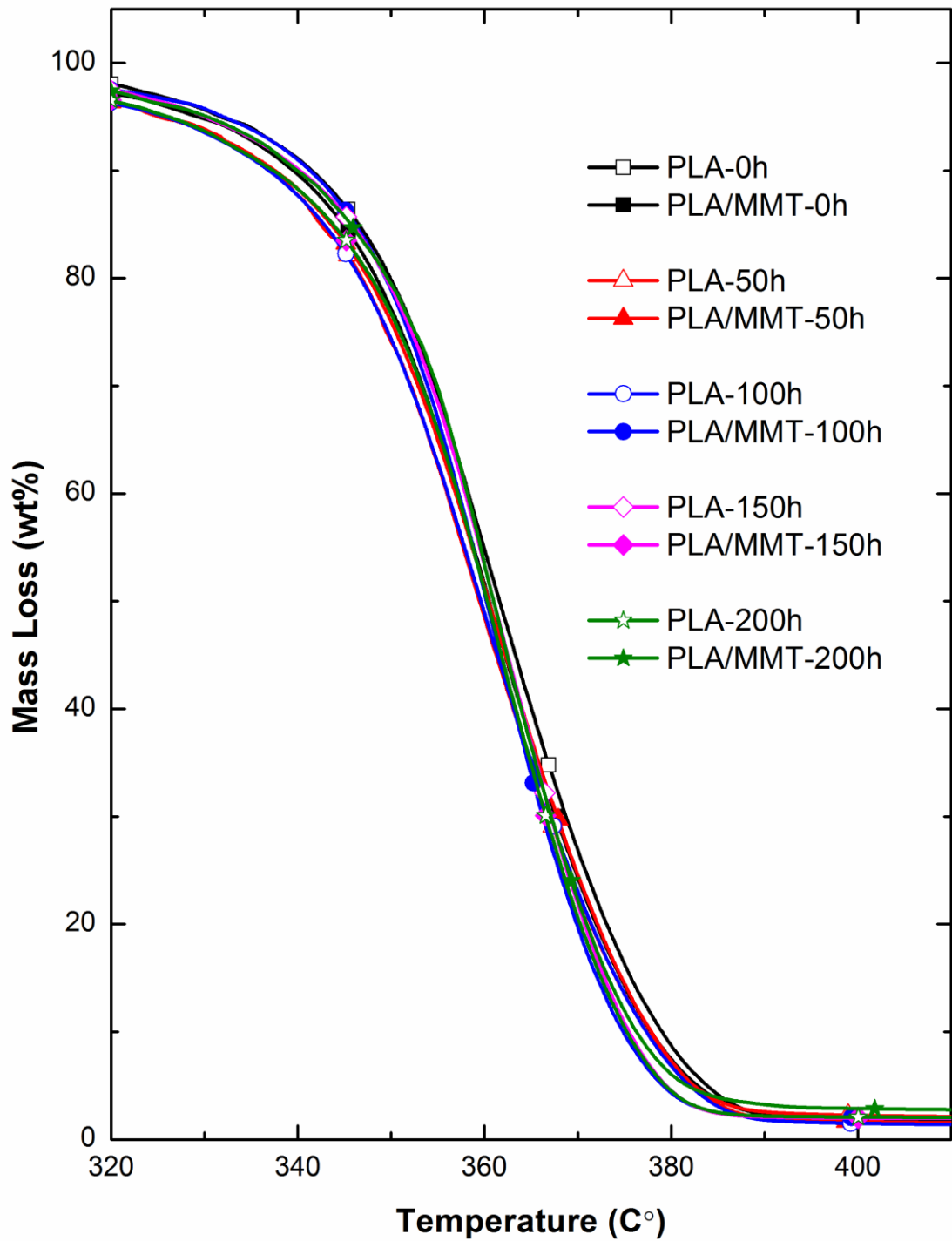


Figure 3.21 Effects of accelerated weathering periods on the thermogravimetric curves of the specimens.

CHAPTER 4

CONCLUSIONS

The main conclusions drawn from the two different parts of this thesis can be summarized as follows:

(i) Effects of MMT Content and MA Compatibilization

- XRD analysis indicated that MMT layers were intercalated successively by the macromolecular chains of PLA, in which d_{001} gallery distance increased from 1.8 nm to 4.79 nm. TEM analysis also revealed that certain level of exfoliation was also present.
- IR analysis pointed out that there could be interaction between the hydroxyl end groups of PLA and the hydroxyl groups present on the surfaces of MMT layers plus in the structure of its organic modifier. After MA compatibilization these interactions were via the oxygen of the carbonyl groups of MA.
- Bending and tension tests showed that due to the composite stiffening and strengthening mechanisms, use of MMT reinforcement increased the modulus and strength values of PLA. For instance, the highest improvement in flexural modulus was 27% by the use of 2 wt% MMT; while it was 7% increase in the flexural strength with 1 wt% MMT. Use of MA compatibilization resulted in no further improvements in the modulus and strength values.

- Ductility measurements in terms of %strain at break (ϵ_f) and K_{IC} , G_{IC} fracture toughness tests indicated that due to the shearing and composite toughening mechanisms; use of MMT resulted in very significant improvements. For example, 1 wt% MMT resulted in more than 6 times increase in ϵ_f value, while 31% and 85% increases in K_{IC} and G_{IC} values, respectively. After MA compatibilization these improvements were much enormous, this time the increase in ϵ_f was more than 22 times, while in K_{IC} and G_{IC} values 70% and 119%, respectively.
- DSC and TGA analyses revealed that incorporation of MMT with and without MA compatibilization have almost no effect on the glass transition and melting temperatures, and also in the thermal degradation temperatures of the neat PLA. The only difference observed in DSC was certain decreases in the cold crystallization temperature of PLA matrix; which was not effective to increase crystallinity amount of PLA.

(ii) Effects of Accelerated Weathering

- XRD diffractograms between 2θ of 1° - 8° indicated that even after accelerated weathering period of 200 h, no change was occurred in the 4.79 nm gallery distance of intercalated MMT layers, i.e. weathering parameters used in this study resulted in no change in the intercalated nanocomposite structure.
- XRD diffractograms between 2θ of 5° - 25° indicated that due to the very fast cooling rate during injection molding, neat PLA and the matrix of MMT nanocomposite specimens were mainly amorphous. However during weathering, UV irradiation cycles taking place at 70°C and the shorter chains of PLA due to chain scission actions of degradation mechanisms provided sufficient energy and time required for the conformational mobility of PLA chains to crystallize.

- CIELAB color space parameters and photographs indicated that variation in the color of specimens occurred mainly during the first 50 h accelerated weathering, in which colorless transparent neat PLA became white; while semitransparent glossy yellowish color of PLA/MMT became opaque pale yellow. Further accelerated weathering periods resulted in only very slight changes.
- IR spectrometry and molecular weight (M_w) measurements via SLS spectrometry revealed that degradation mechanisms of photolysis, photooxidation and hydrolysis during each stage of accelerated weathering resulted in chain scission in the PLA structure, which reduced M_w of PLA matrix from 3.7×10^5 down to 0.8×10^5 ; and consequently decreased the mechanical properties of the specimens.
- Mechanical property determinations pointed out that except slight increases during the first 50 h of accelerated weathering due to higher crystallinity; further weathering periods resulted in successive reductions in the modulus, strength, ductility and toughness of the specimens. For example, at the end of 200 h total accelerated weathering, decreases in the tensile strength of PLA and PLA/MMT were 61% and 51%, respectively; and in G_{IC} fracture toughness 37% and 50%, respectively.
- It can be deduced that, after comparing all mechanical properties of neat PLA and its nanocomposite before and after 200 h accelerated weathering, use of PLA with only 1 wt% MMT was extremely beneficial not only for “indoor applications” but also for “outdoor applications”, which was due to the effective nanoscale reinforcing and barrier actions of intercalated/exfoliated MMT layers. For example, flexural strength and G_{IC} fracture toughness were 6% and 85% beneficial before weathering, but after weathering these benefits were 88% and 68%, respectively.

- DSC and TGA thermograms exhibited no significant variation in the transition temperatures and thermal degradation temperatures of neat PLA and PLA/MMT nanocomposite specimens, except higher crystallinity occurred during weathering.

REFERENCES

- [1] L.T. Lim, R. Auras and M. Rubino, “*Processing technologies for poly(lactic acid)*”, **Progress in Polymer Science**, 33, 820–852 (2008).
- [2] N. Tenn, N. Follain, K. Fatyeyeva, F. Poncin-Epaillard, C. Labrugere and S. Marais, “*Impact of hydrophobic plasma treatments on the barrier properties of poly(lactic acid) films*”, **RSC Advances**, 4, 5626 (2014).
- [3] K. Masutani and Y. Kimura, “*PLA synthesis: From the monomer to the polymer*”, in A. Jimenez, M. Peltzer and R. Ruseckaite (Eds.), **Poly(lactic acid) science and technology: Processing, properties, additives and applications**, 1-36 (2014), Royal Society of Chemistry, London, UK.
- [4] D. E. Henton, P. Gruber, J. Lunt and J. Rendall, “*Poly(lactic acid) technology*”, in A. K. Mohanty, M. Misra and L. T. Drzal (Eds.), **Natural fibers, biopolymers and biocomposites**, 527-577 (2005), CRC Press, Florida, USA.
- [5] T. Mekonnen, P. Mussone, H. Khalil and D. Bressler, “*Progress in bio-based plastics and plasticizing modifications*”, **Journal of Materials Chemistry A**, 1, 13379 (2013).
- [6] C. Marega, A. Marigo, V. Di Noto, R. Zannetti, “*Structure and crystallization kinetics of poly(Lactic acid)*”, **Macromolecular Chemistry and Physics**, 193, 1599-1606 (1992)
- [7] P. De Santis, A.J. Kovacs, “*Molecular Conformation of Poly (S-lactic Acid)*”, **Biopolymers**, 6, 299-306 (1968)

[8] H. Balakrishnan, A. Hassan, M. Imran and M. U. Wahit, “*Toughening of Polylactic acid nanocomposites: A short review*”, **Polymer-Plastics Technology and Engineering**, 51:2, 175-192 (2012).

[9] S.C. Tjong, “*Structural and mechanical properties of polymer nanocomposites*”, **Materials Science and Engineering Reports**, 53, 73–197 (2006).

[10] N. Sozer and J. L. Kokini, “*Nanotechnology and its applications in the food sector*”, **Trends in Biotechnology**, 27:2, 82–89 (2009).

[11] E. Ikada, “*Photo- and Bio-degradable Polyester. Photodegradation Behaviors of Aliphatic Polyesters*”, **Journal of Photopolymer Science and Technology**, 10, 265-270 (1997)

[12] S. Bocchini, K. Fukushima, A. Di Blasio, A. Fina, A. Frache and F. Geobaldo, “*Polylactic acid and polylactic acid-based nanocomposite*”, **Photooxidation Biomacromolecules**, 11, 2919–2926 (2010).

[13] A.V. Janorkar, A. T. Metters and D. E. Hirt, “*Degradation of poly(L-lactide) films under ultraviolet-induced photografting and sterilization conditions*”, **Journal of Applied Polymer Science**, 106, 1042-1047 (2007)

[14] M. Kaci, A. Benhamida, L. Zaidi, N. Touati, and C. Remili, “*Photodegradation of poly(lactic acid)/organo-modified clay nanocomposites under natural weathering exposure*”, in C. Silvestre and S. Cimmino (Eds.), **Ecosustainable polymer nanomaterials for food packaging innovative solutions, characterization needs, safety and environmental issues** (2013), CRC Press, Florida, USA

[15] A. Copinet, C. Bertrand, S. Govindin, V. Coma and Y. Couturier, “*Effects of ultraviolet light (315 nm), temperature and relative humidity on the degradation of polylactic acid plastic films*”, **Chemosphere**, 55, 763-773 (2004)

- [16] B.S. Ndazi, “*Characterization of hydrolytic degradation of polylactic acid/rice hulls composites in water at different temperatures*”, **eXPRESS Polymer Letters**, 5: 119-131, (2011)
- [17] M.K. Nampoothiri, R.N. Nair and R.P. John, “*An Overview of The Recent Developments in Polylactide (PLA) Research*”, **Bioresource Technology**, 101, 8493-8501 (2010)
- [18] A.P. Gupta and V. Kumar, “*New Emerging Trends in Synthetic Biodegradable Polymers–Polylactide: A.Critique*”, **European Polymer Journal**, 43, 4053-4074 (2007)
- [19] S.S. Ray and M. Bousmina, “*Biodegradable Polymers and Their Layered Silicate Nanocomposites: In Greening The 21st Century Materials World*”, **Progress in Materials Science**, 50, 962-1079 (2005)
- [20] J. Rhim, S. Hong and C. Ha, “*Tensile, Water Vapor Barrier and Antimicrobial Properties of PLA/Nanoclay Composite Films*”, **LWT Food Science and Technology**, 42, 612-617, (2009)
- [21] I.H. Chang, Y.U. An and G.S. Sur, “*Poly(Lactic Acid) Nanocomposites with Various Organoclays. I. Thermomechanical Properties, Morphology, and Gas Permeability*”, **Journal of Polymer Science, Part B: Polymer Physics**, 41, 94–103, (2003)
- [22] K. Fukushima, D. Tabuani and G. Camino, “*Nanocomposites of PLA and PCL Based on Montmorillonite and Sepiolite*”, **Materials Science and Engineering**, C29, 1433-1441, (2009)

- [23] N.C. Najafi, M.C. Heuzey and P.J. Carreau, “*Poly lactide (PLA)-Clay Nanocomposites Prepared by Melt Compounding in The Presence of a Chain Extender*”, **Composites Science and Technology**, 72(5), 608–615, (2012)
- [24] S.Y. Lee and M.A. Hanna, “*Preparation and Characterization of Tapioca Starch-Poly(Lactic Acid)-Cloisite NA+ Nanocomposite Foams*”, **Journal of Applied Polymer Science**, 110(4), 2337–2344, (2008)
- [25] S.Y. Lee and M.A. Hanna, “*Tapioca Starch-Poly(lactic acid)-Cloisite 30B Nanocomposite Foams*”, **Polymer Composites**, 30(5), 665–672 , (2009)
- [26] M. Pluta, “*Morphology and Properties of Polylactide Modified by Thermal Treatment, Filling with Layered Silicates and Plasticization*”, **Polymer**, 45, 8239-8251, (2004)
- [27] M.A. Paul, M. Alexandre, P. Degee, C. Henrist, A. Rulmont and P. Dubois, “*New Nanocomposite Materials Based on Plasticized Poly(L-lactide) and Organo-modified Montmorillonites: Thermal and Morphological Study*”, **Polymer**, 44, 443–450, (2003)
- [28] S. Bourbigot, G. Fontaine, S. Bellayer and R. Delobel, “*Processing and Nanodispersion: A Quantitative Approach for Polylactide Nanocomposite*”, **Polymer Testing**, 27, 2-10, (2008)
- [29] N. A. Isitman, M. Dogan, E. Bayramli and C. Kaynak, “*The Role of Nanoparticle Geometry In Flame Retardancy of Polylactide Nanocomposites Containing Aluminium Phosphinate*”, **Polymer Degradation and Stability**, 97, 1285-1296, (2012)
- [30] L. Jiang, J. Zhang and M.P. Wolcott, “*Comparison of Polylactide/Nano-Sized Calcium Carbonate and Polylactide/Montmorillonite Composites: Reinforcing Effects and Toughening Mechanisms*”, **Polymer**, 48, 7632-7644, (2007)

- [31] G.X. Zou, X. Zhang, C.X. Zhao and J. Li, “*The Crystalline and Mechanical Properties of PLA/Layered Silicate Degradable Composites*”, **Polymer Science Series A**, 54(5), 393–400, (2012)
- [32] S.S. Ray, K. Yamada, M. Okamoto and K. Ueda, “*Biodegradable Polylactide/Montmorillonite Nanocomposites*”, **Journal of Nanoscience and Nanotechnology**, 3, 503–510, (2003)
- [33] S.S. Sabet and A.A. Katbab, “*Interfacially Compatibilized Poly(lactic acid) and Poly(lactic acid)/Polycaprolactone/Organoclay Nanocomposites with Improved Biodegradability and Barrier Properties: Effects of the Compatibilizer Structural Parameters and Feeding Route*”, **Journal of Applied Polymer Science**, 111, 1954–1963, (2009)
- [34] Y.Y. Leu, Z. A.M. Ishak and W.S. Chow, “*Mechanical, Thermal, and Morphological Properties of Injection Molded Poly(lactic acid)/SEBS-g-MAH/Organo-Montmorillonite Nanocomposites*”, **Journal of Applied Polymer Science**, 124, 1200–1207, (2012)
- [35] E.A. Cumkur, T. Baouz and U. Yilmazer, “*Poly(Lactic Acid)–Layered Silicate Nanocomposites: The Effects of Modifier and Compatibilizer on the Morphology and Mechanical Properties*”, **Journal of Applied Polymer Science**, (2015) DOI: 10.1002/app.42553
- [36] A.K. Mohapatra and S. Mohanty, “*Study of Thermo-Mechanical and Morphological Behaviour of Biodegradable PLA/PBAT/Layered Silicate Blend Nanocomposites*”, **Journal of Polymer and Environment**, 22, 398–408, (2014)
- [37] M. Pluta, J.K. Jeszka and G. Boiteux, “*Polylactide/Montmorillonite Nanocomposites: Structure, Dielectric, Viscoelastic and Thermal Properties*”, **European Polymer Journal**, 43, 2819–2835, (2007)

- [38] L. Jiang, B. Liu and J. Zhang, “*Properties of Poly(lactic acid)/Poly(butylene adipate-co-terephthalate)/ Nanoparticle Ternary Composites*”, **Industrial and Engineering Chemistry**, 48, 7594-7602, (2009)
- [39] C. Zhang, C. Man, W. Wang, L. Jiang and Y. Dan, “*Degradation of Poly(L-lactide) Films under Ultraviolet Irradiation and Water Bath*”, **Polymer-Plastics Technology and Engineering**, 50, 810–817 (2011)
- [40] H. Tsuji, Y. Echizen and Y. Nishimura, “*Photodegradation of biodegradable polyesters: A comprehensive study on poly(L-lactide) and poly(3-caprolactone)*”, **Polymer Degradation and Stability**, 91, 1128-1137 (2006)
- [41] M. Deroine, A. L. Duigou, Y. M. Corre, Y. M. L. Gac, P. Davies, G. Cesar and S. Bruzard, “*Accelerated aging of polylactide in aqueous environments: Comparative study between distilled water and seawater*”, **Polymer Degradation and Stability**, 108, 319-329 (2014)
- [42] H. Shinzawa, M. Nishida, T. Tanaka and W. Kanematsu, “*Accelerated weathering-induced degradation of poly(lactic acid) fiber studied by near-infrared (NIR) hyperspectral imaging*”, **Applied spectroscopy**, 66, 470-4 (2012)
- [43] S. Dopico-García, A. Ares-Pernas, J. Otero-Canabal, M. Castro-López, J. M. López-Vilariño, V. González-Rodríguez and M. J. Abad-López, “*Insight into industrial PLA aging process by complementary use of rheology, HPLC, and MALDI*”, **Polymers Advanced Technologies**, 24, 723–731 (2013)
- [44] H. Tsujia, K. Ikarashia and N. Fukuda, “*Poly(L-lactide): XII. Formation, growth, and morphology of crystalline residues as extended-chain crystallites through hydrolysis of poly(L-lactide) films in phosphate-buffered solution*”, **Polymer Degradation and Stability**, 84, 515-523 (2004)

- [45] M. J. Jo, Y. J. Ryu, J. H. Ko and J. S. Yoon, “Hydrolysis and thermal degradation of poly(l-lactide) in the presence of talc and modified talc”, **Journal of Applied Polymer Science**, 129(3), 1019-1025 (2013)
- [46] M. Gardette, S. Thérias, J. Gardette, M. Murariu and P. Dubois, “Photooxidation of polylactide/calcium sulphate composites”, **Polymer Degradation and Stability**, 96, 616-623 (2011)
- [47] M. Pluta, M. Murariu, M. Alexandre, A. Galeski and P. Dubois, “Polylactide compositions. The influence of ageing on the structure, thermal and viscoelastic properties of PLA/calcium sulfate composites”, **Polymer Degradation and Stability**, 93, 925-931 (2008)
- [48] Y. Liu, W. Chen and H. Kim, “Synthesis, Characterization, and Hydrolytic Degradation of Polylactide/Poly(ethylene glycol)/Nano-silica Composite Films”, **Journal of Macromolecular Science, Part A: Pure and Applied Chemistry**, 49(4), 348-354 (2012)
- [49] G. Gorrasi, C. Milone, E. Piperopoulos, M. Lanza and A. Sorrentino, “Hybrid clay mineral-carbon nanotube-PLA nanocomposite films. Preparation and photodegradation effect on their mechanical, thermal and electrical properties”, **Applied Clay Science**, 71, 49–54 (2013)
- [50] A. Buzarovska and A. Grozdanov, “Biodegradable Poly(L-lactic acid)/TiO₂ Nanocomposites: Thermal Properties and Degradation”, **Journal of Applied Polymer Science**, 123, 2187–2193 (2012)
- [51] C. Mana, C. Zhang, Y. Liu, W. Wang, W. Ren, L. Jiang, F. Reisdorffer, T. P. “Nguyen and Y. Dan, “Poly (lactic acid)/titanium dioxide composites: Preparation and performance under ultraviolet irradiation”, **Polymer Degradation and Stability**, 97, 856-862 (2012)

- [52] S. SolarSKI, M. Ferreira and E. Devaux, “Ageing of polylactide and polylactide filaments”, **Polymer Degradation and Stability**, 93, 707-713 (2008)
- [53] A. Rapacz-Kmita, E. Stodolak-Zych, B. Szaraniec, M. Gajek and P. Dudek, “Effect of clay mineral on the accelerated hydrolytic degradation of polylactide in the polymer/clay nanocomposites” **Materials Letters**, 146, 73–76 (2015)
- [54] W. L. Tham, B. T. Poh, Z. A. Mohd Ishak and W. S. Chow, “Water absorption kinetics and hygrothermal aging of poly(lactic acid) containing halloysite nanoclay and maleated rubber”, **Journal of Polymer and Environments**, 23, 242-250 (2015)
- [55] A. Araújo, G. L. Botelho, M. Silva and A. V. Machado, “UV Stability of Poly(Lactic Acid) Nanocomposites”, **Journal of Materials Science and Engineering B**, 3(2), 75-83 (2013)
- [56] S. Bocchini and A. Frache, “Comparative study of filler influence on polylactide photooxidation”, **Express Polymer Letters**, 7(5), 431-442 (2013)
- [57] L. Zaidi, M. Kaci, S. Bruzard, A. Bourmaud and Y. Grohens, “Effect of natural weather on the structure and properties of polylactide/Cloisite 30B nanocomposites”, **Polymer Degradation and Stability**, 95, 1751-1758 (2010)
- [58] H. Balakrishnan, A. Hassan, M. Imran and M. U. Wahit, “Aging of toughened polylactic acid nanocomposites: Water absorption, hygrothermal degradation and soil burial analysis”, **Journal of Polymers and the Environment**, 19, 863-875 (2011)
- [59] E. Kontou, P. Georgiopoulos and M. Niaounakis, “The Role of Nanofillers on the Degradation Behavior of Polylactic Acid”, **Polymer Composites**, 33(2), 282-294 (2012)

- [60] M. A. Paul, C. Delcourt, M. Alexandre, P. Dege' e, F. Monteverde and P. Dubois, "*Poly lactide/montmorillonite nanocomposites: study of the hydrolytic degradation*", **Polymer Degradation and Stability**, 87, 535-542 (2005)
- [61] J. Derho, J. Soulestin and P. Krawczak, "*Structural evolution of poly(lactic acid)/poly(ethylene oxide)/unmodified clay upon ambient ageing*", **Journal of Applied Polymer Science**, 131, 40426 (2014)
- [62] P. Pluta, M. A. Paul, M. Alexandre and P. Dubois, "*Plasticized poly lactide/clay nanonocomposites. II. The effect of aging on structure and properties in relation to the filler content and the nature of its organo-modification*", **Journal of Polymer Science: Part B: Polymer Physics**, 44, 312-325 (2006)
- [63] S. Gumus, G. Ozkoc and A. Aytac, "*Plasticized and unplasticized PLA/organoclay nanocomposites: Short- and long-term thermal properties, morphology, and nonisothermal crystallization behavior*", **Journal of Applied Polymer Science**, 123, 2837–2848 (2012)
- [64] W. M. Chavez-Montes, G. Gonzalez-Sanchez, E. I. Lopez-Martinez, P. Lira-Gomez, L. Ballinas-Casarrubias and S. Flores-Gallardo, "*Effect of artificial weathering on PLA/nanocomposite molecular weight distribution*", **Polymers**, 7, 760-776 (2015)
- [65] C. Kaynak and Y. Meyva, "*Use of Maleic Anhydride Compatibilization to Improve Toughness and Other Properties of Polylactide Blended with Thermoplastic Elastomers*", **Polymers for Advanced Technologies**, 25, 1622-1632, (2014)
- [66] S.Y. Lee, I. Kang, G. Doh, H. Yoon, B. Park and Q. Wu, "*Thermal and Mechanical Properties of Wood Flour/Talc-filled Polylactic Acid Composites: Effect of Filler Content and Coupling Treatment*", **Journal of Thermoplastic Composite Materials**, 21, 209-223, (2008)

[67] S. Jain, M. Misra, A. K. Mohanty, and A. K. Ghosh, “*Thermal, Mechanical and Rheological Behavior of Poly(lactic acid)/Talc Composites*”, **Journal of Polymer and Environment**; 20, 1027-1037, (2012)

[68] N. Petchwattana, S. Covavisaruch and S. Petthai, “*Influence of Talc Particle Size and Content on Crystallization Behavior, Mechanical Properties and Morphology of Poly (Lactic Acid)*”, **Polymer. Bulletin**, 71, 1947-1959, (2014)

[69] S. Molinaro, M. C. Romero, M. Boaro, A. Sensidoni, C. Lagazio, M. Morris and J. Kerry, “*Effect of Nanoclay-Type and PLA Optical Purity On The Characteristics of PLA-Based Nanocomposite Films*”, **Journal of Food Engineering**, 117, 113–123, (2013)

[70] S.W. Hwang, S. B. Lee, C. K. Lee, J. Y. Lee, J. K. Shim, S. E. M. Selke, H. Soto-Valdez, L. Matuana, M. Rubino and R. Auras, “*Grafting of maleic anhydride on poly(L-lactic acid). Effects of physical and mechanical properties*”, **Polymer Testing**, 31, 333-344, (2012)

[71] M. Mehrabzadeh, M. R. Kamal and G. Quintanar, “*Maleic Anhydride Grafting Onto HDPE by In Situ Reactive Extrusion and Its Effect On Intercalation and Mechanical Properties of HDPE/Clay Nanocomposites*”, **Iranian Polymer Journal**, 18 (10) , 833-842, (2009)

[72] E.W. Fischer, H.J. Sterzel and G. Wegner, “*Investigation of Structure of Solution Grown Crystals of Lactide Copolymers by Means of Chemical Reactions*”, **Colloid and Polymer Science**, 251, 980-990, (1973)

[73] J. Zhang, K. Tashiro, H. Tsuji and A. J. Domb, “*Disorder-to-disorder phase transition and multiple melting behavior of poly(l-lactide) investigated by simultaneous measurements of WAXD and DSC*”, **Macromolecules**, 41, 1352-1357 (2008)

[74] J. Zhang, K. Tashiro, A. J. Domb and H. Tsuji, “Confirmation of disorder a form of poly(*l*-lactic acid) by X-ray fiber pattern and polarized IR/Raman spectra measured for uniaxially-oriented samples”, **Macromolecular Symposia**, 242, 274-278 (2006)

[75] I. Kaygusuz and C. Kaynak, “Influences of Halloysite Nanotubes on Crystallisation Behaviour of Polylactide”, **Plastics, Rubber and Composites: Macromolecular Engineering**, 44 (2) , 41-49 (2015)